Materials Today Sustainability 35 (2026) 101383

Contents lists available at ScienceDirect

Materials Today Sustainability

journal homepage: www.journals.elsevier.com/materials-today-sustainability

Reactive extrusion of reeds (*Phragmites australis*) and production of binder-less foam insulator

Ainu Voipio [a,d], Veikko Möttönen [b], Kristiina Lång [c], Tapani Vuorinen [d], Anuj Kumar [a,*]

[a] Natural Resources Institute Finland (Luke), Production Systems, Viikinkaari 9, Helsinki, 00790, Finland
[b] Natural Resources Institute Finland (Luke), Production Systems, Yliopistokatu 6B, Joensuu, 80100, Finland
[c] Natural Resources Institute Finland (Luke), Bioeconomy and the Environment, Tietotie 4, Jokioinen, 31600, Finland
[d] Department of Bioproducts and Biosystems, Aalto University, Vuorimiehentie 1, Espoo, 02150, Finland

ARTICLE INFO

Keywords:
Common reeds
Hydrothermal treatment
Multi-screw reactive extrusion
Binder less
Bio-foam
Thermal insulator

ABSTRACT

The construction and packaging industries are heavily dependent on petroleum-derived products such as polyurethane (PU) and polystyrene foams, as well as energy-intensive mineral and rock wool. Their low thermal conductivity, moisture resistance, long-term durability, low cost, and wide availability have made these materials difficult to substitute. However, in recent years, there has been growing demand for sustainable, renewable, and environmentally friendly alternatives to petroleum-derived products, driving considerable research and development in this area. Several natural materials, including wood fiber, hemp fiber, and rice and wheat straw fibrous panels, have been utilized for thermal insulation applications in the construction sector. These materials offer notable advantages such as low thermal conductivity, high porosity, and tuneable mechanical properties, alongside inherent biodegradability and a reduced carbon footprint. Nevertheless, significant challenges remain, particularly with respect to moisture resistance, thermal stability, and continued reliance on fossil-derived binders in their production. In the present work, binderless foams based on common reed (*Phragmites australis*) were produced using hydrothermally treated and reactive extrusion-processed reed fibers. The resulting foams demonstrated thermal conductivity comparable to that of PU and polystyrene foams, along with adjustable density. Moreover, the reed foams exhibited excellent dimensional stability under both water immersion and high humidity conditions. This work also provides a comprehensive characterization of the chemical composition of common reed before and after various treatments, as well as the process know-how required for binderless foam production.

1. Introduction

According to some estimates, almost 50% of energy in Europe is used for heating and cooling buildings [1–4]. In recent years, efforts have been made to reduce the heat losses in buildings through insulating exterior walls, building bases, roofs, attics and by changing windows with lower transmission losses [1]. Similarly, minimization of heat losses in old buildings via refurbishment has significantly improved the heating efficiency [2]. Several types of fossil-based thermal insulating materials, such as expanded polystyrene (XPS), extruded polystyrene, polyurethane foams (pMDI), phenolic foams, have provided excellence performance during the service life in buildings [5,6]. Mineral wool and rock wool, covering almost 60% of the total thermal insulation material market, have been considered suitable replacements of the fossil-based materials [7]. However, the production of mineral and rock wool production is an energy intensive process, and the largely unrecyclable products of inorganic materials like rock wool, glass wool and slag wool are landfilled [8–10]. Some high performance insulation materials, such as gas insulation panels, aerogels, vacuum insulation materials, nano insulation materials and dynamic insulation material, are recently emerging the market, but the cost of such materials are high in large scale building applications [5].

Renewable materials such as wood pulps, straw, plant-based fibers, etc., are considered an alternative to fossil materials in production of thermal insulators for building application [5]. Bio-based insulation materials can help in mitigating depletion of nonrenewable resources, also contributing to the passive control of indoor air conditions (temperature and humidity) via the hygroscopicity of lignocellulose [11].

* Corresponding author.
E-mail address: anuj.kumar@luke.fi (A. Kumar).

https://doi.org/10.1016/j.mtsust.2026.101383
Received 29 October 2025; Received in revised form 7 May 2026; Accepted 12 May 2026
Available online 15 May 2026

Wood fiber based light weight flexible panels and foams are produced industrially [12–15]. However, due to the tough competition for wood among the wood product industry, pulp and paper production, energy sector and biorefineries, alternative biomass sources need to be explored for production of biobased thermal insulators. Due to its porous structure and large scale commercial production, hemp shiv or hurd is considered to be an alternative to wood as a renewable source for thermal insulator production [16–18]. Several other renewable biomass feedstocks, such as rice husk [19], wheat husk [19], date palm wood fibers [20] and sugarcane bagasse, have been also explored in production of thermal insulators [20] Plants growing in unmanaged or marginal lands, i.e. sea shores, lake shores and other wet land areas, are mostly unutilized at large scale [21–25].

Phragmites australis also known as common reed is a wetland plant from the grass family *Poaceae*, genus *Phragmites*. It is widely distributed worldwide [26], and especially in Europe, Middle East and America [27]. Reeds have been used by humans in roofs thatching since the last ice age [28]. Reeds are also used in insulating materials, reed and granulate panels, and pulp and paper production. In energy sector reeds are combusted or converted to biogas or other biofuels. In agriculture sector reeds are used as fodder for animals and as a fertilizer/compost for nutrient recovery. However, processing the reeds into fiber and utilized in production of panels has not been explored in detail like hemp-based plant materials. Production of bio-foam is very rarely reported in existing literature. The most common way to produce the thermal insulator from plant base straw raw materials is via thermomechanical pulping (TMP) defibrillation process to get fibers and produce flexible and rigid panels like conventional wood fibers-based panels [29–32]. TMP process has its limitations in terms of size and dimension of fibers and large size fibers could not fit specially for foam production. Producing foams using straw raw materials is hardly reported earlier in scientific literature.

Extrusion of plant straw sits at the intersection of physical deconstruction of a complex biological material, and the processing demands of modern materials engineering. Its value lies in collapsing what were historically multi-step, multi-vessel processes bleaching, drying, compounding into a continuous, tunable operation that can be adapted for outputs ranging from defibrated pulp for fiberboards to nanofibrils for high-performance biocomposites. However, more advanced reactive extrusion with multi-screw is a continuous, fast method to depolymerize and defibrillate plant straw into soluble biochemicals and fibers with residence times of less than 2 min [33,34].

The present study aims to depolymerize and defibrillate the common reeds into micro-size fibers using a novel single step process using multi-screw reactive extrusion (REX) and produce the binderless reed foam insulator. Two types of foaming processes were adopted to produce foams with different densities. Further, the addition of a thermomechanical pulp (TMP) of reed was also explored to enhance the porosity or other properties of the foams. All the relevant chemical and physical properties of the raw materials and the produced foams were measured thoroughly with a focus on the insulation performance of the foams.

2. Materials and methods

2.1. Materials

The reed was harvested from a lakeshore in Litti municipality, Finland, in March 2023. The reed received were coarsely chopped (ca. 5 cm) and air-dried for storage and transportation purposes. Additionally, a thermomechanical reed pulp (TMRP) prepared with traditional disk refining was also used. All chemicals used in the analysis were laboratory grade.

2.2. Pressurized hot water extraction (PHWE)

The PHWE of the reed was carried out at pilot scale with extraction instrument Uutinkoneikko 1-09114 (Viitos-Metalli Oy, Finland), which has a reactor volume of 360 l. A 29,4 kg batch of reed was extracted at liquid-to-solid ratio of 1:10 with settings of 160 °°C at 10 bar for 30 min. The temperature of the mass on the lower part, where the temperature probe was installed, varied between 135 and 155 °C. The yield of the extracted fibres (ER) was ca. 82 %. The extraction chamber with the raw material and wet reed after extraction can be seen in Fig. 1.

2.3. Reactive extrusion of common reed

The common reed biomass both untreated and PHWE treated were first grounded to ≤1 mm particle size using Cutting Mill Pulverisette (model 19) (Fritsch GmbH, Germany). The reed biomass was first premoistened to ca. 72% dry solid content and homogenized using Electrolux Professional K70 TRK Mixer. Feeder rates were determined for both samples by measuring the feeding amount at three different screw-speeds of the feeder in three replicates. The extrusion was carried out with Planetary Roller Extruder L-WE 30 (Entex, Germany). DDSR20 feeder (Kubota Brabender technologie GmbH, Germany) was connected to the side-feeder perpendicular to the main extrusion barrel and utilized HNP Microsysteme for water side feeding. The extruded material was discharged through a 10 mm die at the end of the barrel. The main parameters of the extrusion for each sample after reaching stable production of extrudate samples can be seen in Table S1 and Table S2. Samples were collected after the system had been stable for 5 min. The extrusions were carried out at 130°°C. This temperature was deemed high enough to allow the softening of lignin leading to defibration even though initially the goal was set at 150° °C. The feeding rate was adjusted to keep the pressure at an adequate level to avoid rapid vaporization of water and blowout of the material at the discharge. The torque of the process was 50-70% for UR and 35-50% for ER. The difference was mainly attributed to the lower final solid content of ER and, to some extent, the softness of ER feed (Fig. 2).

2.4. Foam preparation

The reeds foams were produced with a targeted density <200 kg/m^3 with solid content range of 6-18%. Two foaming agent hydrogen peroxide (H_2O_2) and sodium dodecyl sulphate (SDS) were used in preparation of foam recipes as dissipated in Table 1. Additionally, thermomechanical reed pulp (TMRP) was also used to see impact on the performance on foam behavior.

First, the extruded reed (UER or EER) was diluted with water to the target dry solid content, the foaming agent was added and mixed to obtain a wet foam, which was poured into a square metal wire container

Fig. 1. The extraction reactor of PHWE filled with common reed (left) and wet extracted reed (right).

Fig. 2. Reeds after extrusion. Extracted reed with darker color is on the left and untreated on the right.

Table 1
Final foam recipes at optimized initial dry solid contents for the two foaming methods.

Sample	Foaming agent	Solid content	Additives (wt% of solid)
UER1	H_2O_2	12 %	TMRP 5%
UER2	SDS	7 %	TMRP 5%
UER3	H_2O_2	12 %	-
UER4	SDS	7 %	-
EER1	H_2O_2	12 %	TMRP 5%
EER2	SDS	7 %	TMRP 5%
EER3	H_2O_2	12 %	-
EER4	SDS	7 %	-

(10 cm × 10 cm x 15 cm) lined with tissue paper and taped at the bottom to reduce leaking of low solid content samples (Fig. 3).

When foaming with peroxide, 50% H_2O_2 and the extruded reed suspension were mixed in 1:5 vol ratio and then poured into the wire container. The decomposition of peroxide (scheme 1) led to spontaneous foaming by the released O_2 gas formation which continued for ca. 10 min.

$$2H_2O_2 \longrightarrow 2H_2O + O_2 \uparrow \quad \text{(Scheme 1)}$$

After foaming, the sample was kept at 130 °C for 2 h, after which the temperature was lowered to 70-100 °C until the foam was dry. SDS foams were prepared by diluting the extruded reed to the dry solid content 1 g/l SDS solution, and then mixing with a laboratory blender for ca. 3-4 min. The mixture was then quickly poured into the container and placed in the oven at 130 °Cfor 2 h and later dried at 70-100° °C.

2.5. Analysis methods

For analysis, the untreated and extracted reed sample was first milled into smaller pieces with a Cutting Mill Pulverisette by Fritch and then grinded to a powder with an IKA A 10 pulveriser for chemical analysis. For extra fine powder needed for XRD and XPS analysis, the ball milling instrument Mixer Mill MM400 by Retch was used when needed. Extruded reeds were freeze-dried before chemical analysis and thermally dried before XRD and XPS analysis.

2.5.1. Fiber analysis

Fiber analysis was carried out with the Valmet Fiber Image Analyser FS 5, equipped with an ultrahigh-definition camera. As the measuring range of the instrument is only up to 7 mm, milled samples were used for untreated and extracted reed. As the extruded reeds contained mainly very small particles, the measuring range of 0–7 mm was used with the program "MFC," which is utilized for micro sized fibres. However, the instrument also gives ISO 16065-2-compliant results, which calculate the values from over 0.2 mm fibres only. Half a teaspoon of material was first mixed with approximately 500 ml of water in a blender and then diluted by eye to near the suitable concentration. The instrument then

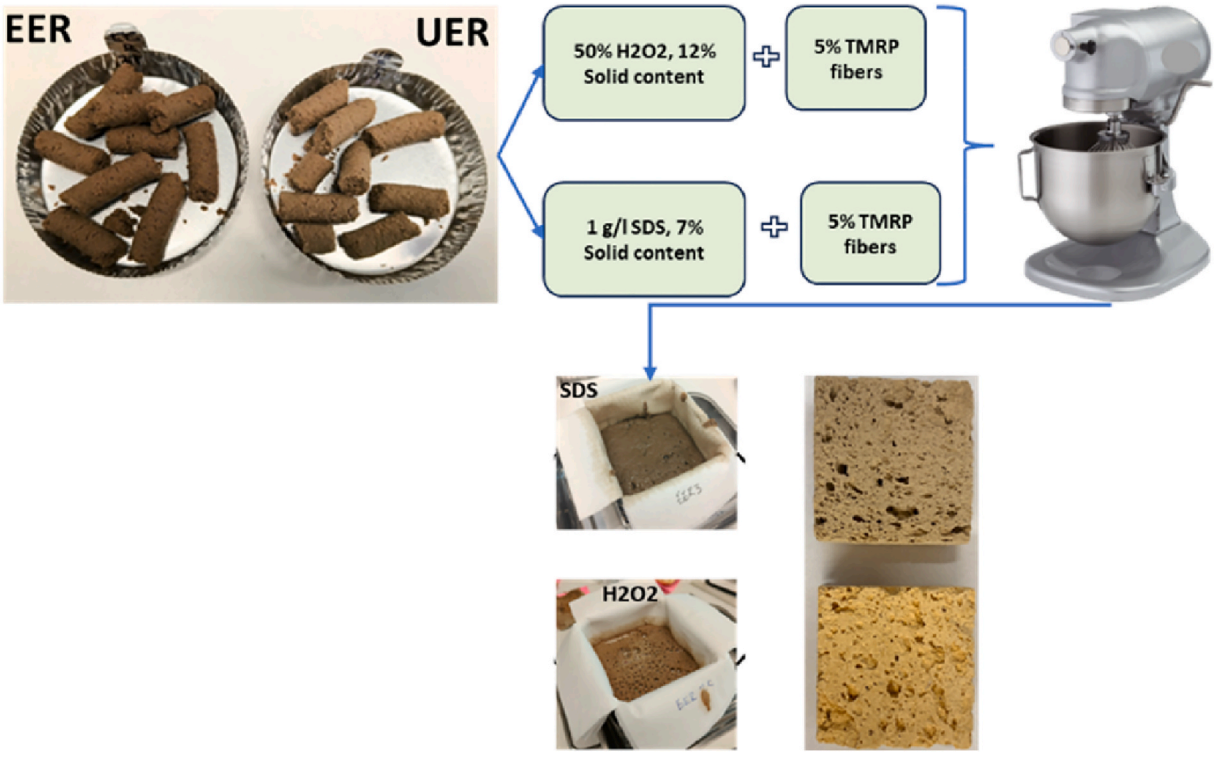

Fig. 3. The process of foam preparation with two different foaming agents, SDS and H_2O_2. After foaming the samples were poured into the metal wire containers, peroxide foams (upper picture) sat there for 10 min before oven and SDS foams were immediately placed in the oven.

diluted the solution automatically to 3 mg/l and analyzed multiple fibre properties with an optical high-resolution camera that captures magnified pictures of the fibres passing through the camera interface. Results including arithmetic average fibre length (l(n)), length-weighted average fibre length (l(l)), weight-weighted average fibre length (l(w)), length-weighed width (w), curl percentage, and amount of fines were obtained.

2.5.2. Crystallinity index

X-ray diffraction (XRD) measurement to determine crystallinity index (CrI) after each treatment step was carried out with PAN analytical X'Pert Pro MPF Alpha 1, with Cu monochromator, κα1. The instrument was run with 45 kV and 40 mA in reflection mode with a sample stage spinning 8 revolutions per minute to capture as representative spectra of the sample as possible. The sample was scanned in 2θ angles from 5 to 60° at a scan speed of 1.33 °degree/min. The crystallinity index was calculated from the peak intensities following the widely used empirical formula:

$$CrI\ (\%) = ((I200\text{-}Iam)/I200)*100$$

I200 is the peak forming from crystalline part of the cellulose around 2θ angle of 22° while Iam is the amorphous hump before the crystalline peak around 16°.

2.5.3. Thermal stability and ash content

Thermal gravimetric analysis (TGA) to determine the thermal stability of the untreated reed (UR), extracted reed (ER), untreated extruded reed (UER), extracted extruded reed (EER), and two examples of foam samples, one made with SDS and TMP fibres and one made with 10% CMC with H2O2, was carried out with the TGA 5500 by TA instruments. The 8–10 mg of samples were heated from 30 °C to 600 °C with a heating rate of 10 °C/min. Additionally, ash content was analyzed with TGA701 by Leco (St. Joseph, MI, USA) by heating from 30 °C to 550 °C, as it has the possibility for a larger sample size (1-2 g) to get more representative results of UR, ER, UER, and EER.

2.5.4. Chemical composition

The chemical composition analysis including the extractive amount and composition, hemicellulose amount and compounds and amount of cellulose and lignin were performed as described below. The dry solid content was measured with Ohaus MB 90 Moisture analyser, with two replicas for each sample.

The extractives were extracted using the Extreva ASE Accelerated Solvent Extractor using ASE 350/150 cellulose extraction filters. Around 1 g of dry untreated reed (UR), extracted reed (ER), untreated extruded reed (UER) and extracted extruded reed (EER) with two replicas for each were weighted in the 22 ml cells. Solvents used for the extraction were hexane, acetone-water with ratio of 95:5 (v:v) and water. Temperature was 80 °C and run time 3 times 5 min with flow rate of 4.4 ml/min. The amount of extractives was determined gravimetrically by taking 20 ml of hexane ex-tract liquid or 10 ml of the other extracts, which were all diluted to 100 ml, and then drying in the oven at 105 °C overnight and weighed to get the dry extract amounts for each. The total extractive amount was calculated by adding up the extractive amounts extracted by each solvent and dividing by the dry weight of the sample. The extractives were further processed by adding 1 ml of an internal standard containing 0.02 mg/ml of heneicosanoic acid (i.e. 21:0 fatty acid) and 0,02 mg/ml of betulinol in methyl tert-butyl ether (MTBE) and silylating them for gas chromatography mass spectrometry (GC-MS) analysis.

GC-FID was done with GC-2010 by Shimadzu with Zebron Zb-1 30 m column with injector temperature of 260 °C, a total flow of 49.3 ml/min, and a column temperature of 100 °C. The FID detector was operated at 290 °^{o}C with a makeup gas flow rate of 30 ml/min, a hydrogen gas flow rate of 40 ml/min, and an air flow rate of 400 ml/min. Lignin amount was analyzed according to the common Klason lignin method described, for example, in Laboratory Analytical Procedure by the National Renewable Energy Laboratory (NREL) of the U.S. Department of Energy. The soluble lignin's absorbance was measured with an UV-Vis spectrometer at 240 nm, and the absorptivity constant of 25 lg-1cm-1 recommended for bagasse in the report by NREL was used as an estimation of common reed's absorptivity constant. Compounds were identified using internal libraries for typical extractives in biomasses and quantified with integration method using internal standards.

Hemicelluloses were analyzed by acid methanolysis using anhydrous HCl. This method does not hydrolyze cellulose to any higher degree, so hydrolyzed sugars originate from non-cellulosic compounds, i.e., hemicelluloses and pectin [30]. Cellulose was analyzed by total hydrolysis with 72% sulfuric acid, which was neutralized after the hydrolysis with BaCO3 using bromocresol green as an indicator. Two standards were prepared for each analysis. For cellulose analysis, cotton linters by Sigma Aldrich were treated same as the samples, and 1 ml of 1 mg/ml of sorbitol in in methanol-water (9:1 v/v) was used for hemicelluloses, evaporating it and then treating it the same as the samples except for staying a shorter amount of time in the oven. For hemicellulose analysis, 4 ml, and 1 ml of internal standard of 0,1 mg/ml resorcinol and sorbitol in methanol-water (9:1 v/v) were added to the samples and standards, respectively. 5 mg/ml sorbitol was used as an internal standard for cellulose analysis and 1 ml of it was added to both samples and standards. Both hemicellulose and cellulose analysis samples and standards were dried completely with heating blocks and nitrogen flow and vacuum oven. All of them were then silylated for gas chromatography-flame ionization detector (GC-FID) analysis.

2.5.5. FTIR

Fourier transform infrared spectroscopy (FTIR) measurements were performed with the IRPrestige-21 by Shimadzu equipped with the attenuated total reflection (ATR) sample holder. The spectra were acquired in absorbance mode with a resolution of 4 cm-1 using 50 scans and a spectral range of 400–4000 cm-1. Apodization was applied using the SqrTri-angle function, and the obtained spectra were analyzed to identify functional groups and compounds in the samples by referencing to literature values.

2.5.6. X-ray photoelectron spectrometry (XPS)

The measurements were performed at Aalto University with a Kratos AXIS Ultra DLD X-ray photoelectron spectrometer (XPS) using a monochromated AlKα X-ray source (1486.7 eV) run at 100 W. A pass energy of 80 eV and a step size of 1.0 eV were used for the survey spectra, while a pass energy of 20 eV and a step size of 0.1 eV was used for the high-resolution spectra. Photoelectrons were collected at a 90° take-off angle under ultra-high vacuum conditions, with a base pressure typically below 1 x 10-9 Torr. The diameter of the beam spot from the X-ray was 1 mm, and the area of analysis for these measurements was 300 μm × 700 μm. Both survey and high-resolution spectra were collected from three different spots on each sample surface to check for homogeneity and surface charge effects. Average values from all three spots on each sample were used to calculate the elemental composition of the samples.

2.6. Characterization of reed foams

2.6.1. Density of foams

Density was measured by measuring the dimensions of the refined piece of sample from multiple points with a calliper in each direction and weighing the sample with an analytical balance. The volume of the sample was calculated based on its shape and dimensions, and density is the weight of the sample divided by its volume.

2.6.2. Microscopic analysis

Olympus light microscopy with 3D imaging capabilities was used to capture images of foams and see how the longer fibres are embedded in

the matrix of the foams. Some simple pore size measurements were also carried out.

Scanning electron microscopy (SEM) of reed foams is carried out using Hitachi S-4800, Field Emission Scanning Electron microscope (FESEM). The foams specimens trimmed to small size and fixed on aluminium sample stub with carbon & copper tapes and coated with 2 nm layer of gold. Measurement parameters used. working distance- about 8 mm; acceleration voltage- 3 kV; emission current - 7 μA and images captures at different magnifications.

2.6.3. Water uptake by foams

The behavior of samples in water and their water uptake was investigated by submerging pre-weighed and pre-measured sample pieces in water for 24 h. After removal, the change in mass (g) and thickness swelling (mm) were recorded. The samples were subsequently dried at 105 °C overnight, after which measurements were taken again to determine whether any material had been lost in the water. This immersion-drying cycle was then repeated once more. Any observations regarding floating or visible disintegration (crumbling) of the samples were also noted throughout the process.

2.6.4. Moisture absorption of foams

The long-term water absorption capacity of the samples was determined in climate chamber Vötsch VCL 4010 (Vötsch Industrietechnik GmbH, Germany) under standard conditions, T = 22 °C, RH 90%. Approximately 10 g of the sample from the foams was initially collected and dried for two days at 60 °C to remove the free water before placing them in the climate chamber. The weight increase of the samples under standard conditions was monitored until their mass no longer increased after approximately three weeks.

2.6.5. Porosity of foams

The Brunauer-Emmett-Teller (BET) analysis was carried out with TriStar II 3020 by Micromeritics. The oven dry empty sample tube weight, weight with sample before nitrogen block drying, and final dry weight were measured with an analytical balance in 5 replicas, and the average value was used as the sample amount in the measurement. The sample density was entered according to the previous measurements. Nitrogen and helium were used as an absorbing gas. The instrument measures the amount of gas absorbed at different pressures at constant temperature and calculates the Barrett-Joyner-Halenda (BJH) pore volume and average pore width from the absorption and desorption isotherms. It also calculates the average surface area and other parameters using the widely used BET equation.

2.6.6. Compression strength of foams

The compression strength of foams was determined using the universal material testing machine Zwick Z050 (ZwickRoell GmbH, Ulm, Germany) equipped with 2.5 kN load cell. Compression test was carried out at the speed of 3 mm/min to 50% deformation and the compression strength, σm (MPa), was calculated as follows:

$$\sigma_m = F_m / A_0,$$

where F_m is the maximum force, in newtons (N) and A_0 is the initial cross-sectional area of the specimen, in square millimetres (mm^2).

2.6.7. Tensile test perpendicular to the surface of foams

Internal bonding of the foams was measured by a tensile strength perpendicular direction of the foam surface. The test followed the standard testing method BS EN 1607:2013 [35]. Reed foams (n = 5 per sample group) were cut into approximately 30 mm × 30 mm x 9 mm specimens and mounted between aluminum plates using epoxy resin adhesive. The specimens were conditioned at 23 °C and 60% relative humidity for overnight before testing. Tensile tests were performed using a universal testing machine at a constant crosshead speed of 1.5 mm/min. The maximum tensile force (Fm) was recorded at failure. The tensile strength perpendicular to the faces (σ_{mt}) was calculated using the following formula:

$$\sigma_{mt} = F_{mt}/(l*b)$$

where: σ_{mt} is the tensile strength in kilopascals (kPa), F_{mt} is the maximum tensile force in kilonewtons (kN), l and b are the length and width of the specimen in meters (m). The reported tensile strength is the mean value of five measurements. Specimens exhibiting any signs of adhesive failure were discarded.

2.6.8. Thermal conductivity of foams

C-Therm thermal conductivity analyzer (TCi) (Fredericton, NB, Canada) was used the evaluate the thermal conductivity of the foams. The method utilizes a modified transient plane measurement method, where a controlled electric current is applied to the sensor's spiral heating element, generating a localized heat source. Simultaneously, the sensor's guard ring activates to establish a one-dimensional heat flow path between the primary sensor coil and the sample. The resulting temperature rise at the sensor-sample interface induces a change in the voltage drop across the sensor element. By monitoring the rate of temperature increase (as reflected in the sensor's voltage), the thermal conductivity of the sample is determined.

3. Results

3.1. Chemical composition and properties of reeds

The obtained chemical composition of the untreated, extracted and both extruded reeds samples are presented in Table 2. According to the literature the chemical composition of reed varies with cellulose between 33 and 51% (w/w), hemicellulose 20-28 %(w/w), lignin 10- 24% (w/w), extractives 2-10% (w/w) and ash 3-9% [36]. The composition of raw material results matches quite well with the literature results, though hemicellulose amount seems to be slightly larger as dissipated in Table 2. The variation in hemicellulose content may be attributed to the different growth properties like location, nutrition, harvesting time and weather conditions during growth. The Klason lignin content was 9.7% for the un-treated sample (UR) and 7.9% for the extracted sample (ER). Similarly, the acid-soluble lignin content was 2.9% for UR and 2.4% for ER. Ash content is in the range of results reported before.

The cellulose amount decreases a little after extrusion, due to the mechanical forces of extrusion disrupt the crystalline structure of cellulose. Hemicellulose content does not seem to be affected much, though the extracted extruded sample shows a slight decrease. Relative lignin content, however, rises radically, almost doubling. This can be explained by hornification of cellulose at elevated temperatures during the extrusion, causing incomplete swelling during the sulfuric acid treatment. The unreactive cellulose will then be analyzed as Klason lignin, causing excessively high value. Lower extractives and cellulose amounts also contribute to the higher relative lignin amount. Extractive amounts decrease radically due to extrusion, the heat and mechanical forces release them from the structure and as a lot of them are acids they might react in the medium, or volatile compounds might vaporize during the process. Further, the detailed analysis of extractives and carbohydrates compounds were also carried out, and the relevant identified extractives and their average values are presented in Table 3. Overall, the untreated sample has higher extractive amount, but some specific acids show higher values for PHWE sample (ER). This might be due to high temperature converting acids during the extraction as the amounts are relatively small and only two repetitions were made.

The concentration of xylose was between 225 and ~260 mg/g in different phases of reeds processing (Fig. 4). During PWHE extraction the concentration of most monosaccharides decreased slightly, as a liquid phase containing sugars was collected during the extraction.

Table 2
Chemical composition (% of dry matter) of the untreated (UR), extracted (ER), untreated extruded (UER) and extracted extruded (EER) reeds.

Sample	Cellulose %	Hemicellulose %	Total Lignin %	Extractives %	Ash %	Sum
UR	43.8 ± 7	31.9 ± 0.6	12.6	4.2 ± 0.5	3.8 ± 0.1	96.3
ER	39.1 ± 1	32.6 ± 0.9	10.4	2.7 ± 0.1	2.8 ± 0.05	87.6
UER	34.4 ± 0.2	31.7 ± 0.7	23.8	0.95 ± 0.0	3.7 ± 0.01	94.6
EER	35.7 ± 0.5	27.9 ± 0.9	23.4	0.63 ± 0.5	3.5 ± 0.02	91.1

Table 3
The identified extractives and their average amounts in the reed at different stages of processing. Standard errors not presented for clarity and due to them being quite small.

Extractives summary	*UR AVG (mg/g)*	*ER AVG (mg/g)*	*UER AVG (mg/g)*	*EER AVG (mg/g)*
Aromatic Compounds				
Vanillic acid	0.0004	-	-	-
p-Coumaric acid	0.0054	0.001	0.0019	0.0026
1-Guaiacylglycerol	0.0008	0.0008	-	-
1-Syringylglycerol	0.0016	0.0007	0.0008	0.0011
Glucuronic acid	0.0007	-	-	-
Sitosterol	0.002	0.0051	0.0036	0.0036
Fatty Acids				
Palmitic acid	0.0044	0.0068	0.005	0.0045
Linoleic acid	0.0005	0.0005	0.0017	0.0009
Vaccenic acid (trans-11-18:1)	0.0007	0.0016	-	-
Oleic acid	-	0.0009	0.0027	0.0018
Elaidic acid (trans-9-18:1)	-	0.0002	0	0.0018
Stearic acid	0.0022	0.0015	0.0036	0.0021
Arachidic acid	-	0.0003	0.0014	0.0008
Behenic acid	-	0.0003	0.0022	0.0018

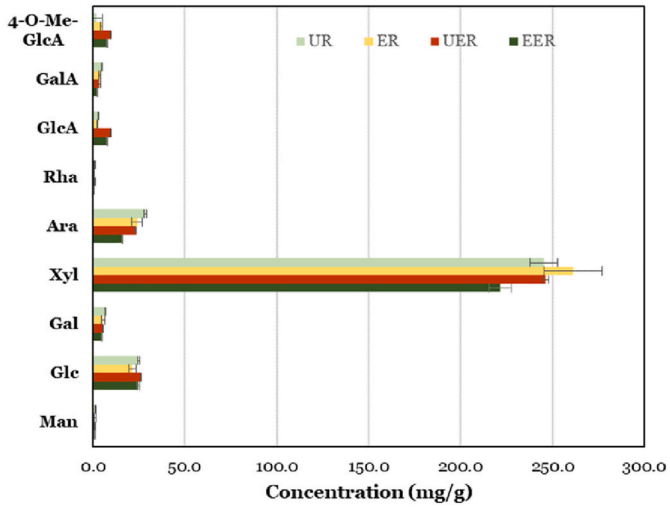

Fig. 4. The concentration of sugar compounds in untreated (UR), extracted (ER), untreated extruded (UER) and extracted extruded (EER) reed. Sugar compounds: Mannose (Man), glucose (Glc), galactose (Gal), xylose (Xyl), arabinose (Ara), rhamnose (Rha), glucuronic acid (GlcA), galacturonic acid (GalA) and 4-O-methyl-glucuronic acid (4-O-Me-GlcA).

However, the decrease is xylan and its substituent, 4-O-methyl-glucuronic acid, which shows an increase after extraction. This is likely due to enhanced xylan solubility due to slight degradation of lignin facilitated by the extraction process, as can be seen in Table 2. The reduction in lignin content improves accessibility to xylan within the plant cell wall during the analysis extraction step [37]. Reactive extrusion overall decreases the sugar amounts similarly to extraction, especially the pectin derived sugars, galacturonic acid, galactose, and arabinose, which show similar behaviour as with extrusion suggesting pectin degradation at high temperatures in both treatments. For other sugars, the extrusion does not affect the amounts remarkably, except for glucose, which increases slightly due the cellulose degradation, and glucuronic acid and 4-O-methyl-glucuronic acid, which show a slight rise.

3.1.1. FTIR

The decrease of extractives and lignin after extraction is visible in IR spectra (Fig. 5), the double peak of associated to CH_2 or CH_3 groups in extractives ~2850 and 2920 cm^{-1} and their intensity decreased after extraction and the intensity of hemicellulose/lignin related peaks around 1720 cm^{-1} [38]. After extrusion the extractive double peak disappears completely. This most likely reduces the hydrophobicity of the material as these compounds typically enhance it. One small clearly different peak appears, and one peak diminishes in the fingerprint region of the spectra, indicating changes most likely in the hemicellulose structure, as supported by the chemical analysis related to the changes in the monosaccharide amounts, but they could also indicate a deformation in lignin structure [39].

3.1.2. XPS analysis

The relative elemental composition obtained with XPS for reeds biomass at different process steps are shown in Table 4. The C 1s% was relatively unchanged due to the PHWE treatment, the composition of N 1s% and Si 2p% significantly reduced due to the possible dissolution into the hot-water and leached out in the process. On the other hand, O 1s% increased slightly due to dissolution of hemicellulose/lignin in the process that open the cellulosic structure. However, the reactive extrusion significantly reduced the C 1s% and increased the O 1s% in both untreated and PHWE treated reeds, due to the induced mechanical forces, temperature and pressure during extrusion process, altered the chemical and morphological structure of reeds.

Table 5 shows the percentage of different components in carbon-based molecules compared to the total percentage of carbon in the samples. The higher C-C carbon bonds in ER and UR might be related to their higher extractive amounts as extractives contain a lot of carbon chains. Extrusion lowers the silica amount but same does not happen to the extracted sample indicating that PHWE-treatment and extrusion have a similar effect on silica amount and that there is a threshold of silica that stays in the material despite the treatments. Fig. 6 dissipated whole C1s spectrum of reeds samples, the peak intensity areas under C (C-C) is higher in untreated reeds ~60%, compared to ER sample. The percentage of oxygen containing carbon chains such as C(C-O), C(C=O) and C(C-C=O) does not change much due to PHWE treatment.

However, the percentages of area under C(C-O), C(C=O) and C(C-C=O) peaks significantly increased after reactive extrusion process as shown in Table 5 and Fig. 6. This residual silica might be beneficial in thermal insulation applications as it typically improves the thermal resistance of the material. However, it is still unclear if the effect is significant enough to be considered an advantage of common reed as a raw material. In general, the silica amount is in line with the results found in literature [40].

3.1.3. Crystallinity index (CrI)

XRD spectra of reeds with the amorphous hump around 16 degrees of 2θ, and the sharp peak around 22° representing the crystalline part of the cellulose can be seen in Fig. 7. The crystallinity index of untreated

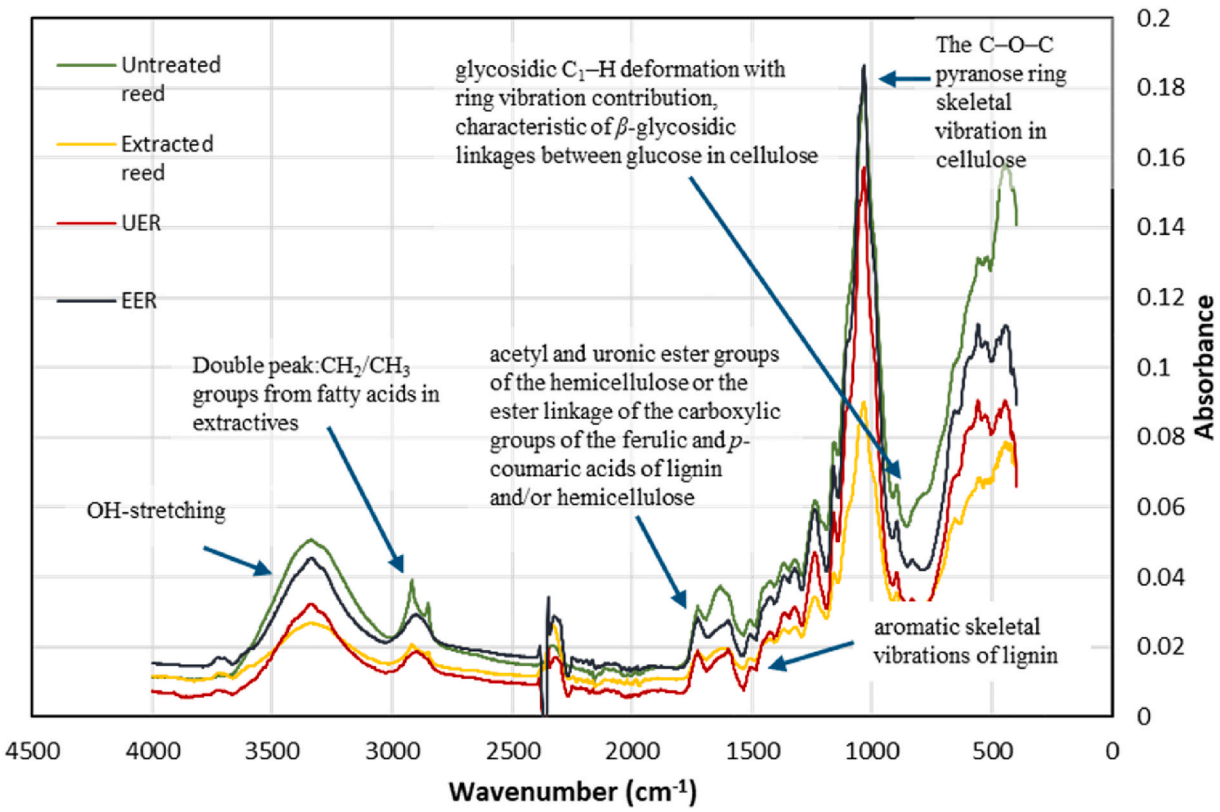

Fig. 5. FTIR graph of untreated, extracted and both extruded reeds. Relevant peaks are marked in the graph.

Table 4
Relative elemental composition of the samples averaged from three positions on the sample surfaces.

Sample	C 1s%	N 1s%	O 1s%	Si 2p%
UR	76.16	1.02	21.53	1.29
ER	76.46	0.48	22.38	0.68
UER	73.21	0.59	25.47	0.72
EER	71.53	0.44	27.29	0.73

Table 5
Relative amounts of the different components of carbon, as compared to the total amount of carbon in the different reeds' samples.

Sample	*C (C-C) %*	*C (C-O) %*	*C (C=O) %*	*C (O-C=O) %*
UR	59.39	30.34	7.27	3.00
ER	53.55	33.67	9.12	3.66
UER	*47.52*	*39.43*	*9.79*	*3.26*
EER	*44.33*	*41.24*	*10.79*	*3.64*

reeds was determined to be 52 % which correlates well with the previous literature values around 50% for untreated reed in literature [41,42]. PHWE process reduced the crystallinity index to 50%. possibly due to the disruption of hydrogen bonds in cellulose. In any case, the relatively high CrI means that common reed can be a good candidate for bio-products as high crystallinity usually indicates good mechanical properties and thermal stability. After extrusion the crystallinity was reduced slightly more resulting untreated extruded reed to have CrI of 46.1% and extracted extruded reed to have CrI of 46.23%. The mechanical forces and pressure and temperature during extrusion are mainly the reason for the decrease and any possible earlier difference between the samples seems to have vanished.

3.1.4. Fiber analysis

The average length-weighted length, ISO standard length-weighted length, width of the fibres and the quantity of fibres analyzed are presented in Table 6. Length/width distribution graph pair of untreated reeds before and after extrusion seen in Fig. 8 also visually show this decrease very clearly. The fibre analysis shows that the fibre dimensions greatly decreased after extrusion both untreated reeds and PHWE treated reeds. It can also be seen that lots of smaller fibres were already present in the un-treated and extracted reeds before extrusion as the length weighed average length differs vastly from the ISO standard length. This is most likely due to milled sample in the analysis and using the whole plant and the flower part having lots of smaller particles and fibres, which causes the average fibre length to decrease when smaller particles are included.

The ISO standard length is smaller than the typical values in the literature, but that is most likely caused by milling done before the analysis, which naturally increases the quantity of smaller fibres. Rough microscopic measurements gave fibre lengths of 1.4 to 5 mm for the raw materials, which conform relatively well with the literature values. The width of the fibres before extrusion decreases clearly as well and this is most likely due the fibre breaking apart due the mechanical forces and as the lignin softens during the process, so some microfibril bundles might detach from the fibre.

3.1.5. Thermogravimetric analysis of reeds materials

Fig. 9 shows the thermal stability of reeds biomass specimens treated with PHWE and reactive extrusion process. The first slight decrease is the excess moisture evaporating mainly from UR and ER samples. The next steep decrease in weight between 255 and 320 °C for most samples is attributed mainly to the hemicellulose degradation and the final drop between 320 and 450-480 °C is principally caused by cellulose degradation. Due to lignin's broad decomposition range and slow degradation, no distinctive lignin-related peak appears throughout the pyrolysis process, but it contributes to the change in residual mass throughout the

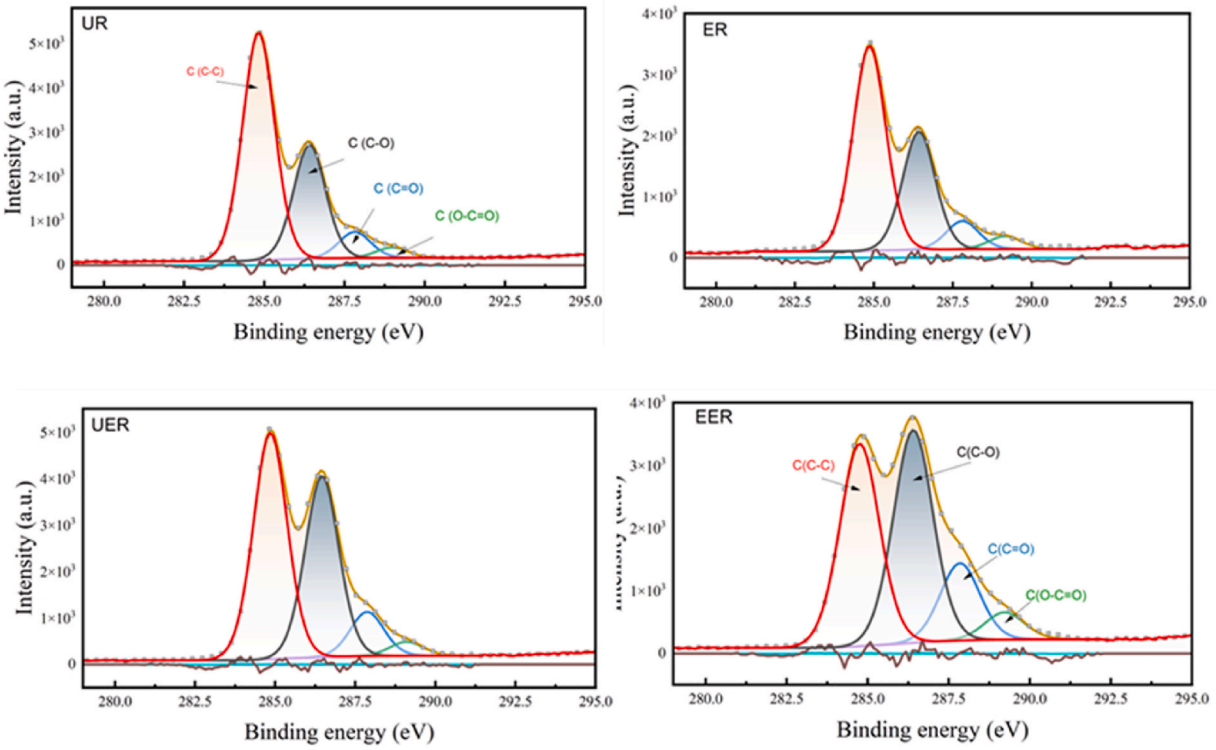

Fig. 6. XPS spectrum of C1s of untreated reed (UR), hot water extracted reeds (ER) and reactive extruded reeds UER and EER.

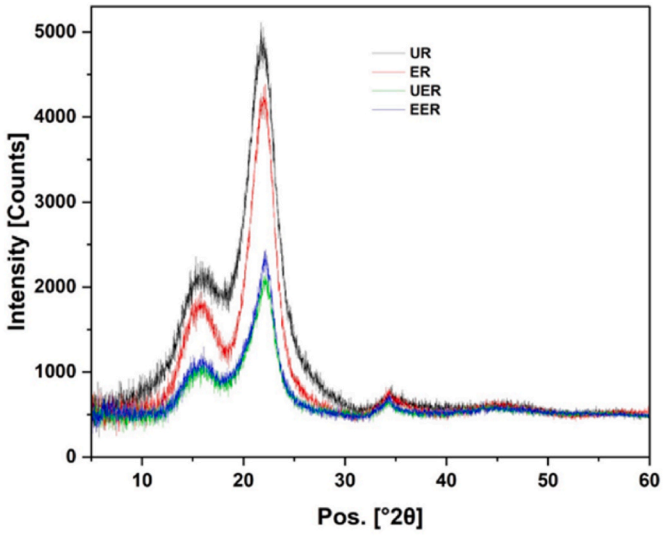

Fig. 7. XRD spectra of reeds specimens processed with treatment stages.

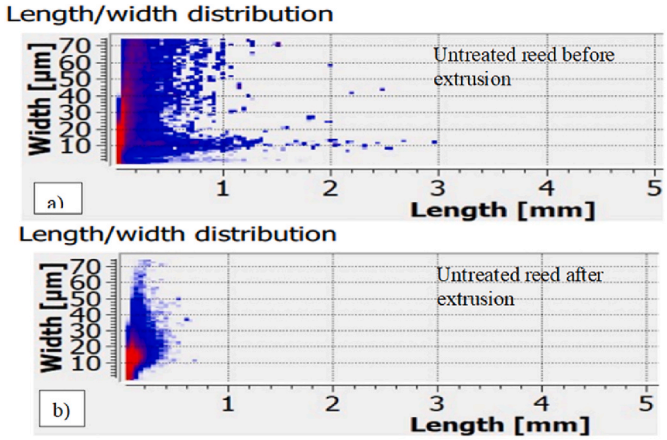

Fig. 8. (a) The length/width distribution of UR before extrusion and b) after extrusion. The radical change could be seen in the size distribution of the fibers after extrusion.

Table 6
Length weighted length (Lc(l)), ISO 16065-2 compliant length-weighted length including fibers over 0.2 mm only and average fibre width and fibre count of untreated (UR), extracted (ER), untreated extruded (UER) and extracted extruded (EER) reed.

Sample	Lc(l) (mm)	Lc(l) ISO (mm)	Fiber width (µm)	Fiber count (n)
UR	0.068	0.53	6.68	2057225
ER	0.068	0.511	6.45	1940721
UER	0.030	0.260	4.05	9647596
EER	0.032	0.272	4.09	9277239

measurement [43].

UR and ER are slightly more stable than extruded reeds as expected as they have undergone minimal treatments, and they have the highest cellulose crystallinity. EER behaves like ER specimens because of hemicellulose degradation rate and slightly lower cellulose decomposition temperature. However, the behaviour of UER is rather peculiar as after the hemicellulose degradation, there is an intense drop in the weight percentage, essentially decomposing entirely and only very small cellulose decrease can be seen after 320°. The onset temperature around 255 °C and the general degradation steps of the TGA curve matches the TGA properties of common reed describe the onset temperature for winter reed to be around 254 °C [43].

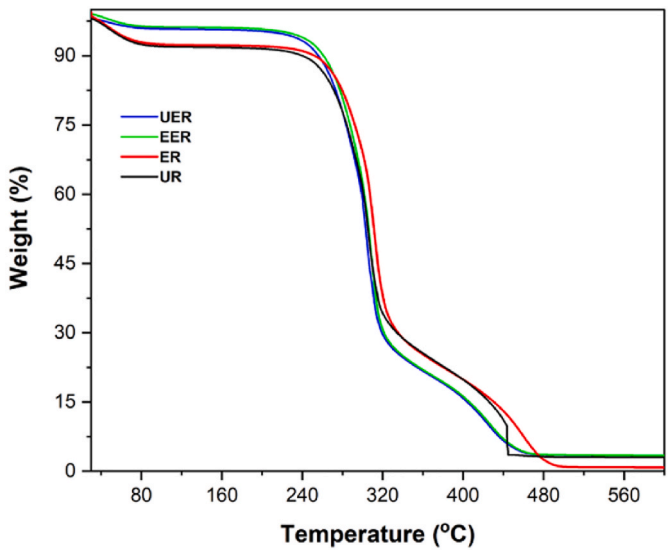

Fig. 9. TGA graphs of raw reeds materials at different processing stages.

3.2. Properties of reeds foams

3.2.1. Density and thermal conductivity of reed foams

The prepared foams showed the densities range between 119 and 240 kg/m^3 (Fig. 10). The foams using SDS as foaming agent showed lower density compared to the H2O2 based foams. Varying the solid content also impacted the density of final foams, H2O2 based foams had a solid content 12%, while the SDS foams content only 7% solid content. Foams produced using untreated reeds showed overall all lower density compared to PHWE treated reeds. Addition of TMRP doesn't show significant impact on final density of foams. UER3 (189 kg/m^3 and EER3 (238 kg/m^3) samples content showed the higher density, as these sample produced using 12% H202 foaming agent only. However, the addition of TMRP to same set (high H_2O_2) reduced the density of foams i.e. UER1 (153 kg/m^3) and EER1 (197 kg/m^3). This trend was not observed for SDS based foams.

Fig. 11 shows the SEM micrographs of reeds foams produced using H_2O_2 foaming agent with and without TMRP fibres. H_2O_2 reeds foam shows the agglomeration of small reeds fibres together in small patches that's created the larger and non-uniform pores due to the aggressive chemical nature of hydrogen peroxide, which is strong bleaching agent. However, after addition of TMRP into mixture, the larger fibre has distributed along with small fibres and reduced the agglomeration

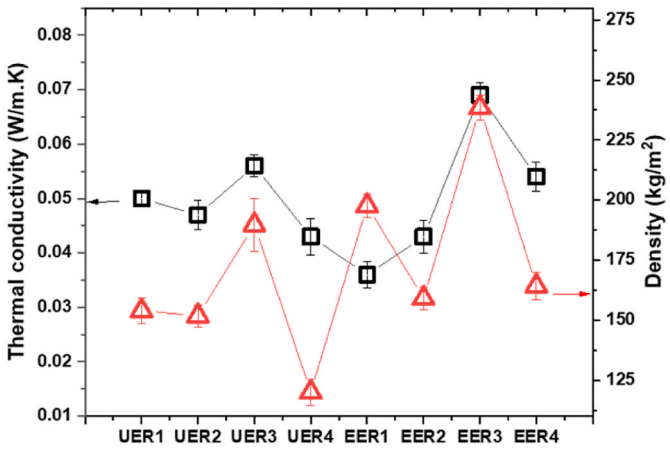

Fig. 10. Densities and thermal conductivity variation between the prepared foams.

(pointed with in Fig. 11). Another, important aspects H_2O_2in the foaming process, it is very aggressively bleached the reeds fibres surface and creates the horn type groves helps to form the stronger bonding between fibres. This could be a reason H_2O_2 foams showed higher compressive and tensile strength compared to SDS foams.

Thermal conductivities of reed foams were between 0.030 W/m•K to 0.069 W/m.K, UER4 has the lowest value and EER3 the highest. As, both these sample also had the lowest and highest densities. for most samples (Fig. 12). The density and thermal conductivity of insulating materials are linearly correlated to each other, if density increased, so the reciprocal thermal conductivity increases [44]. However, this assumption is not entirely true, there are several many factors, which impacted the overall values performance of insulating materials. For bio-based or natural materials, for example open-cell insulation materials which are made from hemp fibres found that a reduction of thermal conductivity with an increase of density due to the condensation inside the sample [45] and sheep wool based insulating materials also showed the same trend with increases density, the thermal conductivity could decrease, but it is temperature depend phenomenon [46]. There are several important factors which impacted the thermal conductivity of natural materials-based insulators, such as moisture content, pore size/volume, and thickness of samples. The reed foams in the present work showed significant linear correlation between foams density and thermal conductivity (Fig. 12) with coefficient of correlation, $R^2 = 0.896$. The addition of TMPR fibres in lower the density and thermal conductivity at least in the case of H_2O_2 based foams such UER1 and EER1 in compared to UER3 and EER3 respectively.

The microscopic images show the differences between different foams with SDS (EER4) and H_2O_2 (EER3) and sample EER3 (SDS) with TMPR fibre, oval circles highlight the uniform presence of TMPR fibres in Figs. 11 and 13, which have similar densities range. TMPR fibres clearly influence the structure of the foam therefore affecting the thermal conductivity by lowering it slightly. The lower end of the obtained thermal conductivities is in the similar approximate as commercially available materials. Most samples are sufficiently below the required 0.06 W/m.K.

3.2.2. Microporosity of reeds foams by BET

The microporosity of reed foams were estimated as average BET surface area, average pore volume and average pore width calculated from the adsorption isotherm (Table 7). SDS is a surfactant, and it creates the uniform slurry of extruded reeds by creating the small pockets of air bubbles during the foaming process and created a uniform cell-wall thickness and wides of pores (see Fig. 14). Reed foams with only with SDS have larger surface area both types of extruded reeds UER4 (~3.49 m^2/g) and EER4 (~2.10 m^2/g); H_2O_2 based reeds foam showed quite similar surface area ~1.24 m^2/g for both types extruded reeds. Addition of TMRP into the foam's matrix, might have affected the uniformity of microporous structure, TMRP behave differently for each type of foaming agent. This is probably related to the foaming process, where SDS foams are physically foamed, leading to possibly thinner pore walls and therefore higher surface area.

According the literature, polyurethane foams also reported the similar specific BET surface area of 1.8-2.8 to m^2/g and the pore volume of the reed foams was much higher the polyurethane has the pore volume reported as 0,0004 cm^3/g [47]. This probably results from the widely varying pore size in reed foams while polyurethane foams tend to have more uniform structure.

3.2.2.1. Moisture absorption. Fig. 15 shows the moisture absorption trends of different reeds foams at 90% RH for a period of one month until the constant weight was achieved. The initial MC% of foams samples varied, the PHWE treated reeds foams showed higher initial MC% compared to untreated reeds as dissipated in Fig. 15. After two weeks of conditioning in 90% RH, the MC% of EER1 specimens increased from

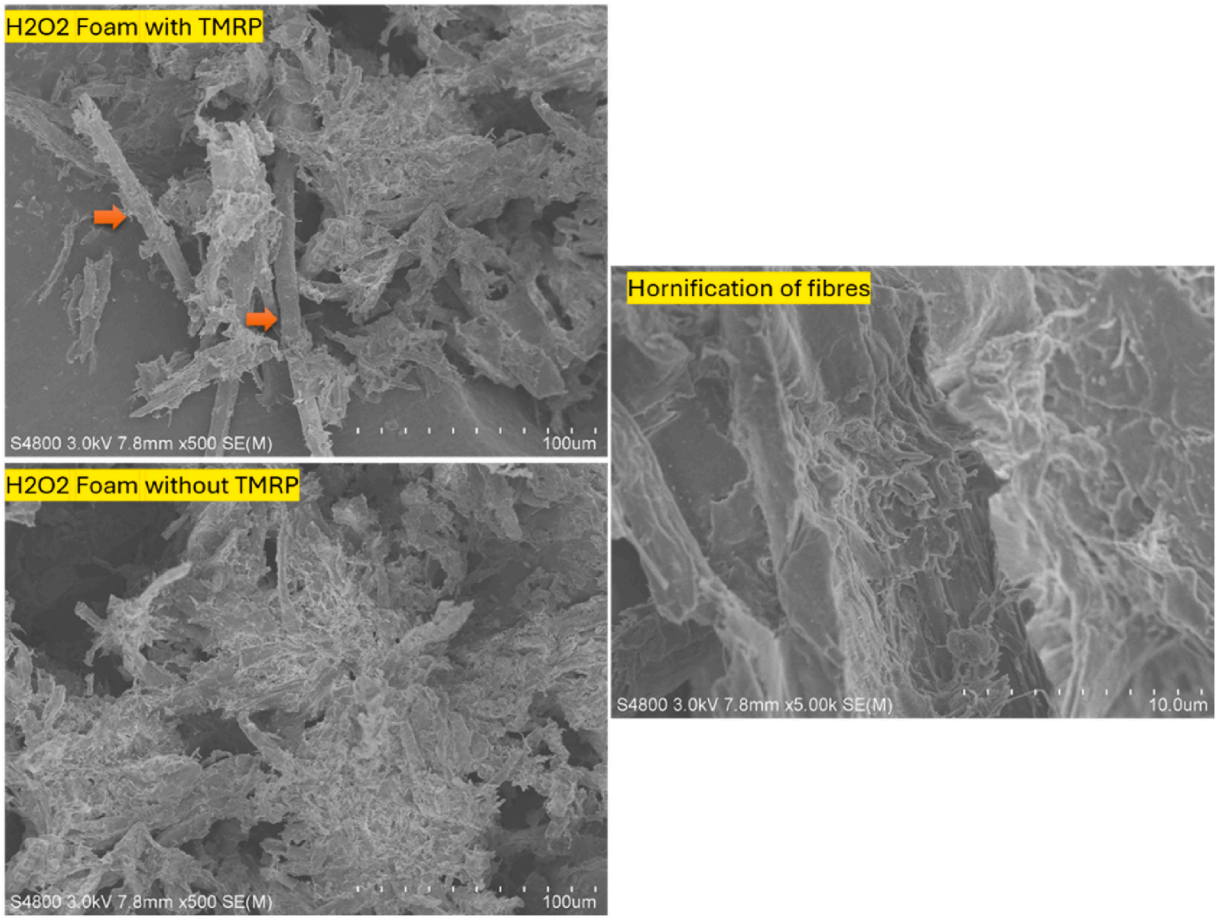

Fig. 11. SEM micrographs of reeds foams produced with H_2O_2foaming agent with and without TMRP fibres.

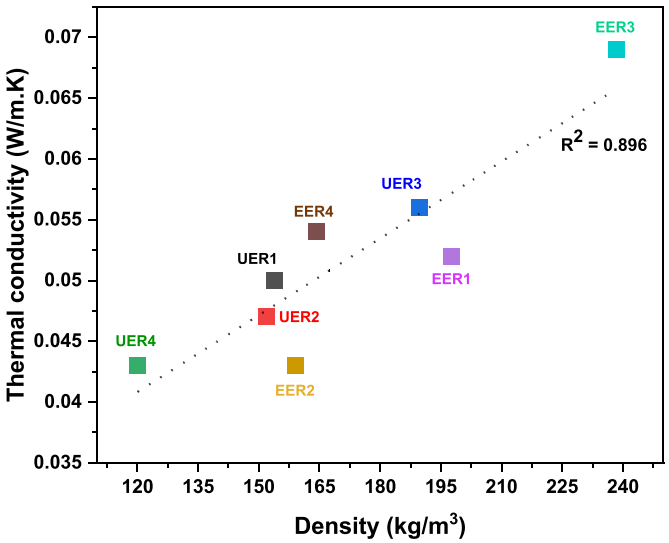

Fig. 12. Correlation between densities and thermal conductivity of the reed foams produced.

3.87% to 10.20%, similar trend was showed by all the EER specimens. On the other side, UER specimens have lower moisture absorption compared to EER, such as UER1 sample initial MC% 3.48% to 5.29% after two weeks conditioning. There is no significant variation was observed in term of foaming agent used in reeds foams production. After, four weeks conditioning 90% RH, showed stable MC%, only difference was the initial treatment of reeds i.e. PHWE treatment impacted the final moisture absorption of reeds foams. This because PHWE treatment removed certain percentage of hemicelluloses, extractives, metals (silicon), from reeds cell-wall and increased hydrophilicity of reeds and its final foam product.

The moisture absorption of the reed foams is a bit higher than for commercial insulations materials that have the absorption at similar humidity around 13% for polyphenolic insulation material and around 6.5% for polyurethane [48]. Common reeds acted as cellulosic materials that tend to absorb more moisture compare to petroleum-based materials. However, the absorbed amount is still acceptable for commercial use and could be improved by further research.

3.2.3. *Water absorption behaviour of reed foams*

The water uptake was measured by immersing reeds foam in water twice with a drying step in-between and after the second wetting. Measuring the weight at different stages of the measurement gives idea of the materials water absorbency and rebound ability after wetting. It can see in Fig. 16, the first immersion showed excessive absorption of water, ranging from 130% to 700% increase for the mass of the sample; all foams stayed relatively intact SDS foams absorbed clearly more water than peroxide foams, most likely due different pore and fibre structure and slightly lower density allowing better permeability. The specimens UER2 and EER3 showed highest water absorption >500% and these foams contains SDS and TMRP fibres. However, samples which does have TMRP in SDS foams also showed higher water absorption to peroxide based foams. They also sunk to the bottom of the container, while peroxide foams floated close to the surface as can be seen Fig. s1. Peroxide foams displayed a yellowing of the water, suggesting the hydrogen peroxide has probably detached some water-soluble

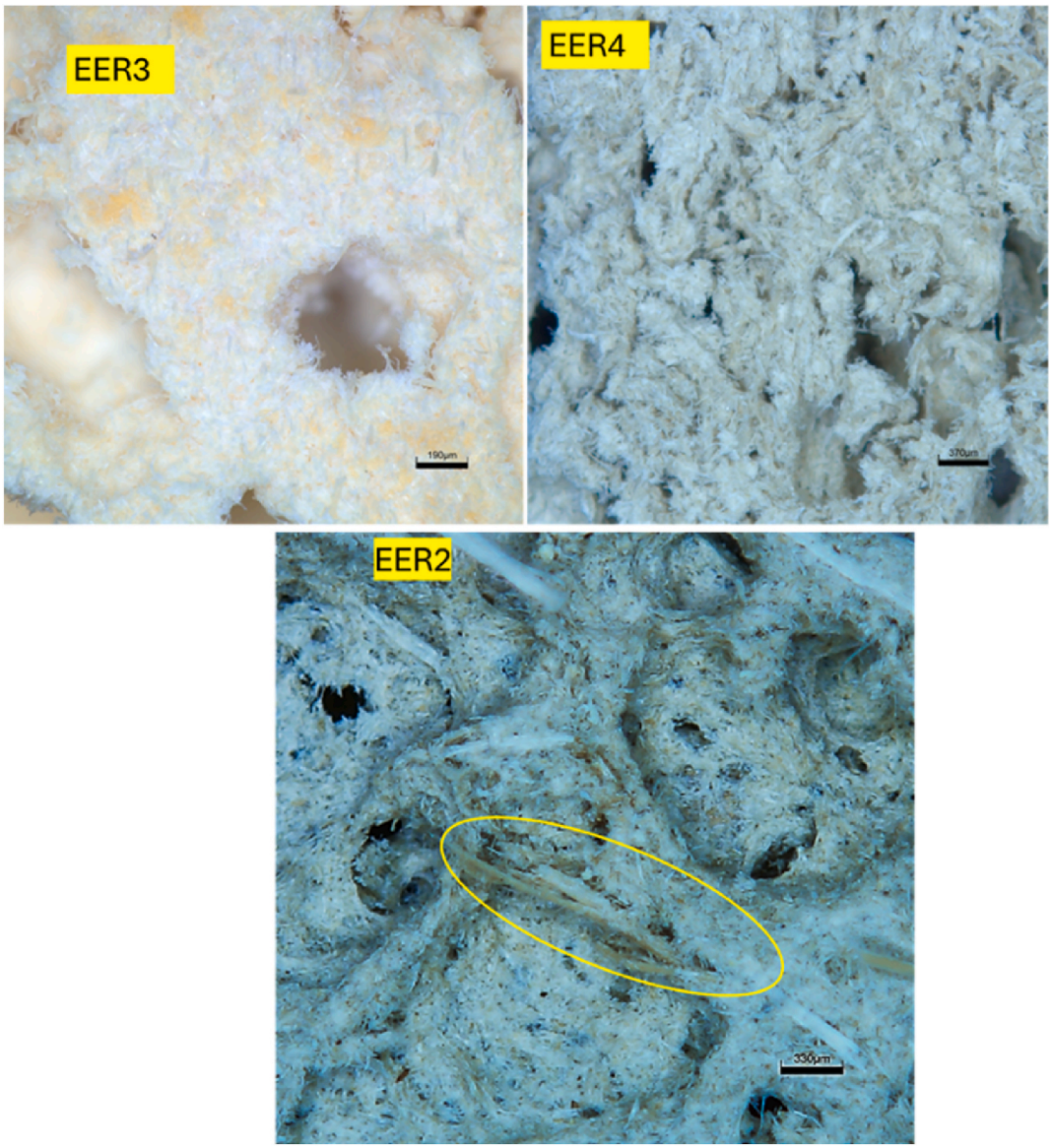

Fig. 13. Microscopic images of EER foams with two different foaming agent EER3 (with H_2O_2), EER2 and EER4 with SDS as foaming agent. EER 2 also reinforced with TMRP fibres.

Table 7
BET surface area, BHJ adsorption pore volume and pore width of reeds foams from adsorption isotherm.

Sample	BET surface area (m^2/g)	Pore volume (cm^2/g)	Pore width (Å)
UER1	0.315 ± 0.088	0.0111 ± 0.0001	83.62 ± 23
UER2	1.63 ± 0.086	0.007 ± 0.0002	185.74 ± 25
UER3	1.24 ± 0.123	0.0060 ± 0.0002	435.54 ± 71
UER4	3.49 ± 0.233	0.010 ± 0.0003	127.79 ± 42
EER1	1.15 ± 0.109	0.0058 ± 0.0002	173.21 ± 42
EER2	0.812 ± 0.088	0.0096 ± 0.0001	100.55 ± 26
EER3	1.22 ± 0.124	0.00506 ± 0.0006	140 ± 27
EER4	2.10 ± 0.231	0.0086 ± 0.0005	157.58 ± 35

chromophores from lignin in the fibres.

However, after drying and second time dipping the water absorption is significantly less for all samples evening out the difference between foaming agents slightly. SDS also floated more as they did not absorb so much water and peroxide foams stayed clear coloured, most likely due leaching of all the chromophores in the first water immersion step. This suggests the drying step at 105 °C, hornifies the fibres, leading to decreased swelling and absorbency of water. This hornification most likely has a larger effect than pore structure and density alone.

3.2.4. *XPS analysis of extruded reeds foams*

High resolution C 1s spectra of reed foams with different foaming agent looks similar. The percentage of C(C-C) peak decreased significantly compare extracted reed and extruded reeds discuss earlier section. On the other side the percentages of oxygen rich C1s peaks increased as shown in Fig. 17 and Table 9.

The percentage data of XPS spectra of different chemical compounds also showed the similar trend C1s% is higher in untreated reed compared to extracted reed and on the other side O1s % is higher in extracted reeds in Table 9. The Si 2p % seems similar in both the type of reeds after extrusion. The UER foam shows slightly lower silica content as can be seen in Table 8 and increased oxygen content. Interestingly the EER foam shows increased silica content compared to raw materials and increased oxygen content. During preparation of raw reed materials, all the parts of reeds plant including leaves and flowers were collected. The silica usually accumulates in that part of the plant and more specific in leaves [49]. Oxygen increase is most likely related to the foaming

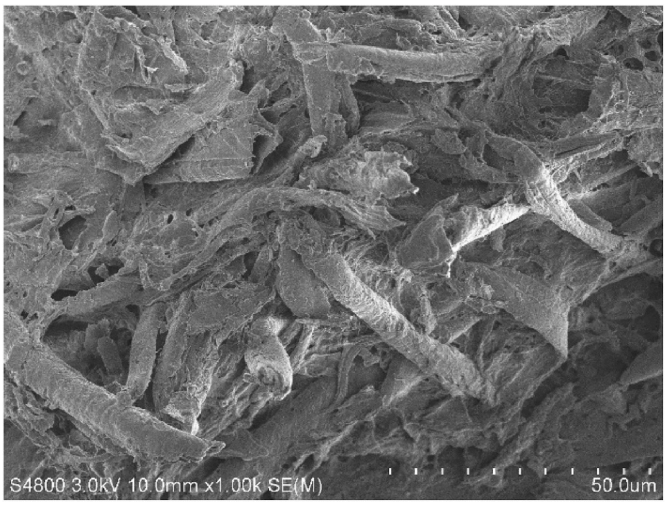

Fig. 14. SEM micrograph of EER4 specimens, which showed uniform packed distribution of extruded reed fibres and uniform pore size.

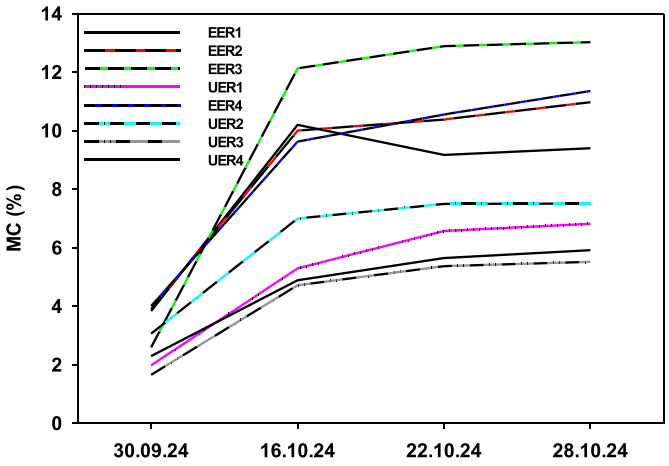

Fig. 15. Hygroscopicity graph of the foams at 22 °C and 90% relative humidity.

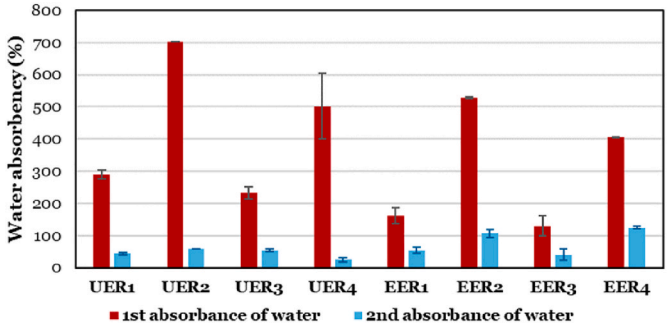

Fig. 16. Water absorbency of reeds foams.

process as there is more surface area available for oxygen-carbon interaction, plus peroxide produces oxygen and oxidizes the foams leading to increase in C=O and O-C=O bonds as seen in Table 9.

In FTIR spectra in Fig. 18, the peak C-H stretching vibration at ~2900 cm^{-1} represents the aliphatic groups found in sugar units of cellulose and hemicellulose and represents the methoxyl groups (-OCH_3) in the lignin structure contribute to C-H vibrations. However, the intensity of this peak reduced compared to raw reeds as shown in Fig. 5 due to the removal of hemicellulose or lignin during fiber extraction or

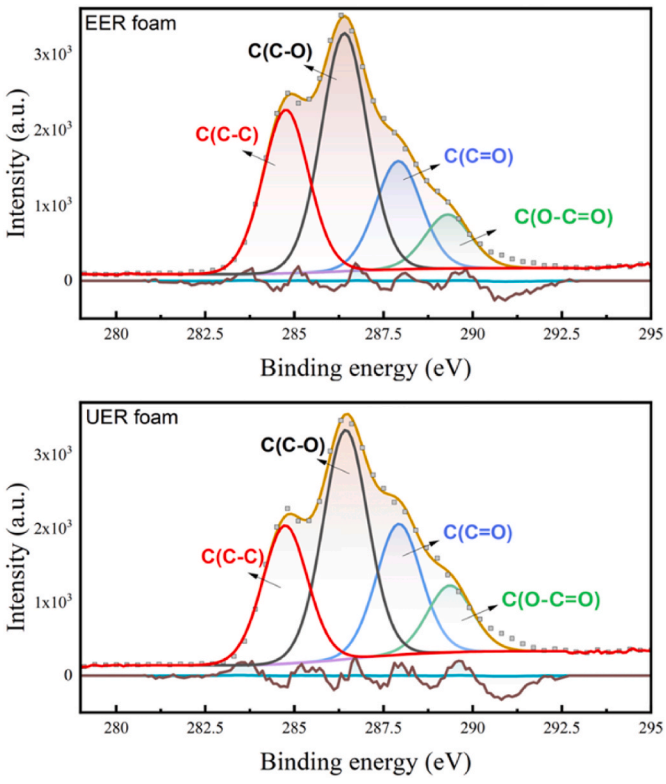

Fig. 17. High resolution spectra of C 1s of the reed foams. UER foam is made with SDS and EER foam with hydrogen peroxide.

Table 8
Relative elemental composition of the samples averaged from three positions on the sample surfaces.

Sample	C 1s %	N 1s %	O 1s %	Si 2p %
UER SDS foam	69,45	0,46	29,45	0,64
EER peroxide foam	67,38	0,27	31,37	0,99

Table 9
Relative amounts of the different components of carbon, as compared to the total amount of carbon in the samples.

Sample	C (C-C) %	C (C-O) %	C (C=O) %	C (O-C=O) %
UER SDS foam	27,37	40,54	20,67	11,42
EER peroxide foam	31,59	43,21	17,04	8,16

chemical treatment. The presence of molecular coordinated water within the SiO2-structure shows at ~1610 cm^{-1} [50], the peaks around ~1500 cm^{-1} to negatively charged silanol (Si-O^-) associated to Si-O^-—Ca^{2+} groups in reeds [51]. The peak at ~1728 cm^{-1} is assigned to the C=O stretching vibration for hemicellulose and pectin content and also indicated the ester linkages between hemicellulose and lignin [52]. The intensity of this peak is higher in peroxide foams compared to SD foams, that means stronger ester bond formation in peroxide foams. This ester carbonyl peak at ~1728 cm^{-1} in FTIR can be directly correlated with XPS C1s mainly with relative peak area of the C(O–C=O) component at ~289.2 eV [53,54]. The peak area (%) of reeds materials prior to the foam formation was between 3 and 3.65% as showed in Table 5; after form formation with SDS and hydrogen peroxide the peak area (%) associated to C(O–C=O) component increased significantly to 11.66% and 8.16% respectively. The broad peak at ~1032 cm^{-1} represents the β [1–4]-glucans associated to the cellulose, lignin and hemicellulose components in both types of foams, and peak ~1051 cm^{-1} linked to the

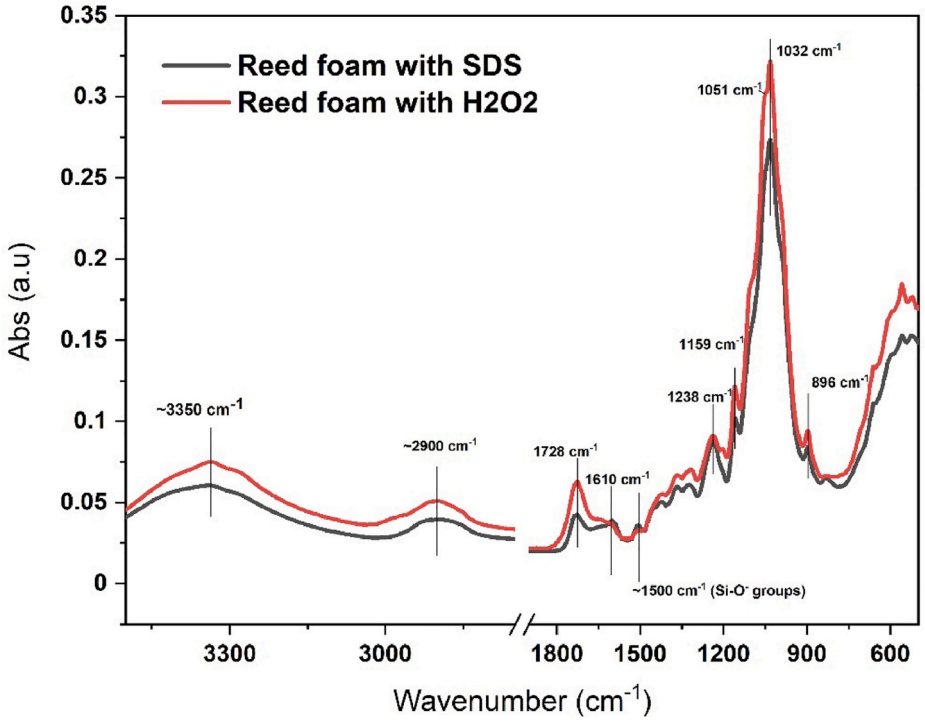

Fig. 18. FTIR spectra of reed foam produced with different foaming agent.

C-O stretch in cellulose and hemicellulose only present in peroxide foams. Similar, outcomes showed in XPS in Table 9, peroxide foam showed percentage of C (C-O) carbon components. The peaks around ~1159 cm^{-1} is linked to the C-O-C vibration between cellulose and hemicellulose; and ~1238 cm^{1} to syringyl ring and C-O stretch in lignin and xylan. Also, one characteristic peak of C-H deformation in β-glucans is present around 896 cm^{-1} in both types of foams.

3.2.5. *Thermal stability of reed foams*

As, Fig. 9 already demonstrated the thermal degradation behaviour of reeds i.e. control sample, hydrothermal treated reeds, and extruded reeds. The SDS foam did not showed any significant difference in thermal stability compared to the raw materials. This thermal stability is on the similar level as petroleum-based PU that has an onset temperature around 251 °C [55], so the SDS foam would be suitable for insulation regarding it's thermal stability.

The peroxide foam, however, shows different behavior with the clearly earlier onset temperature around 150 °C as can be seen in Fig. 19. It has also an earlier drop in the middle of the cellulose degradation curve around 375 °C, suggesting a rapid decomposition of the remaining material. H_2O_2 significantly affects the lignin structure, as it forms free radicals (HOO·, HO·) in addition to molecular oxygen, which all react with lignin in several reaction pathways. Hydroxyl radical can degrade also any other organic material, including cellulose. This is visible in the color change of the foams made with peroxide as well, essentially the peroxide bleaches the foams. This partial delignification and degradation of the biomass lead to lower molecular-weight fractions, therefore leading to lower thermal stability.

3.2.5.1. *Mechanical properties of reed foams*

3.2.5.1.1. Compression strength. The compressive strength of reed foams varies between 0.25 N/mm^2 to 1.32 N/mm^2 at 50% compressive force as shown in Fig. 20. The peroxide samples showed higher compressive strength, because of the higher density and SDS foams EER2 and EER4 show comparable values to peroxide foams EER 1 and EER3 despite having lower density. For UER samples peroxide samples are clearly superior in compression strength, for example if comparing

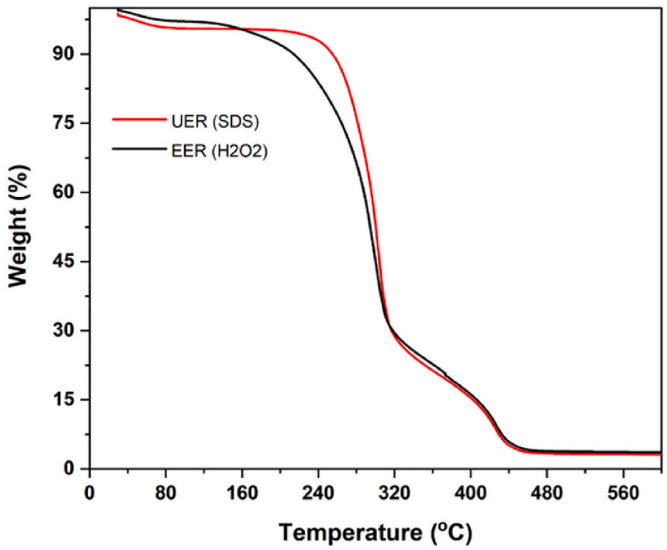

Fig. 19. The TGA curves of two example foams, SDS foam made with UER, and peroxide foam made with EER.

UER2 and UER1 that have the same density and recipe. It can be concluded the peroxide altered the chemical properties of reeds due to bleaching effect.

Addition of longer fibres seem to have minimal effect on the compressive strength and no clear difference between UER and EER, however SDS foams where UER had poorer compression strength. In general, the reed foams had relatively high compressive strength and ductility at 50% deformation ranging from 0.75 to 1 MPa. Typically, compression strength of thermal insulation materials is measured at 10% deformation, and for polyurethane with a density of roughly 100 kg/m3, it has been reported to be around 0.3 MPa [56]. Applying the stress-strain curves and the dimensions of the measured reed samples, a compression strength at 10% deformation in the range of

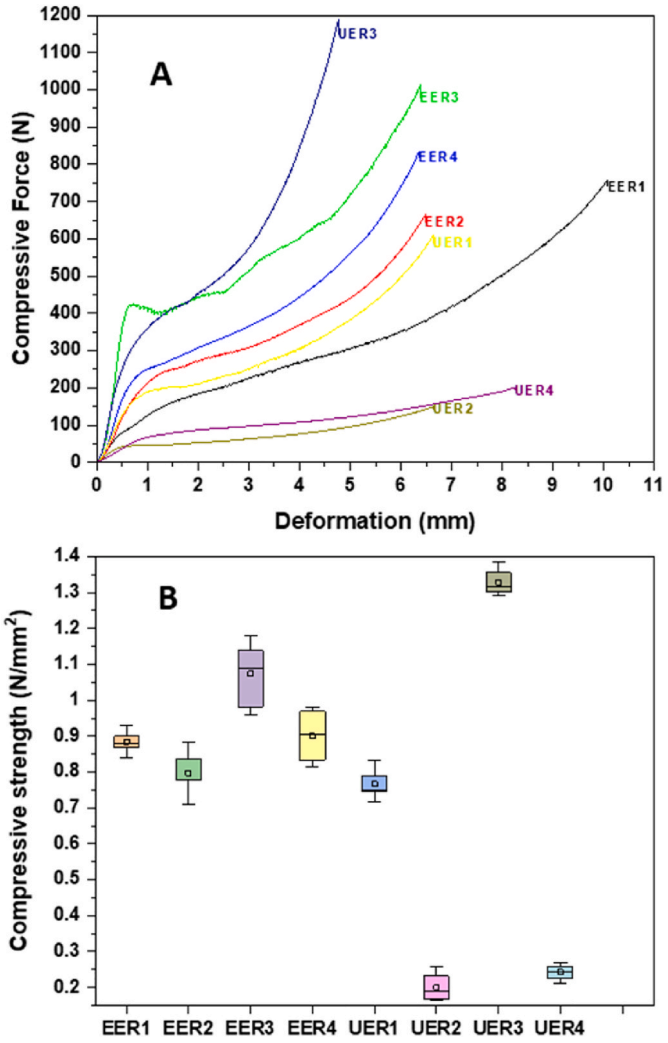

Fig. 20. a) Average compression-deformation curves of the samples. b) A boxplot of the compressive strength at 50% deformation.

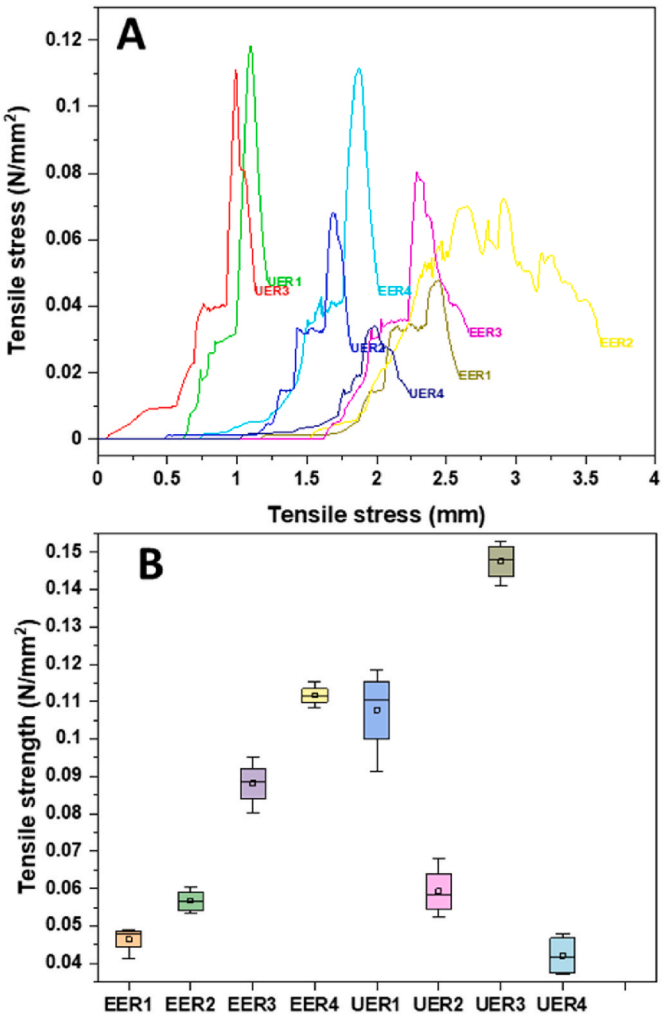

Fig. 21. a) Stress-strain curves of the reed foam samples and b) a boxplot presenting the tensile strength of the samples.

0.07-0.6 MPa is estimated. Other bio-polyphenolic foam [56] with a similar density range as the reed foams in this thesis had compression strengths ranging from 0.09 to 0.7 MPa at 10% compression. Thus, reed foams are equivalent in strength to other bio-based alternatives.

3.2.5.1.2. Perpendicular tensile strength. The tensile strength boxplot (Fig. 21) suggests that the SDS foams have higher tensile strength for EER samples, but the effect is opposite for UER samples. In general, the peroxide foams made with UER have significantly higher tensile strength compared to EER. SDS samples with TMRP fibers perform similarly despite the raw material, but without the longer fibers the EER4 sample has clearly better internal bonding than the UER4 sample.

For most of the peroxide-based foams shows higher maximum force is needed to break compared to SDS foams. However, the breakage was very brittle, and strain was much smaller than for the SDS foams, indicating that the peroxide foams were quite brittle compared to SDS foams. The higher strain of SDS foams suggest higher flexibility and ability to spread the applied force more evenly. For EER samples the SDS seemed to give better bonding than peroxide, but for UER the SDS samples had poorer bonding than peroxide foams. UER peroxide foams performed significantly better than EER peroxide foams. UER SDS foams had similar or poorer tensile strength than EER SDS foams. Addition of longer fibres lowered the internal bonding. Overall, the addition of longer fibres lowers the internal bonding, TMRP fibres disturbs this linkage, possibly by causing larger pores and therefore poorer bonding. The perpendicular tensile strength of industrial grade EPS is 100 kPa [47], from SDS based foams EER4 would meet this requirement. On the other hand, peroxide-based reed foams EER5, UER1 and UER3 exceed this requirement clearly.

4. Discussion

Building construction sector is among the highest emitter of greenhouse gases due to its excessive dependency on Portland cement and fossil derived products. Most of the fossil derived products used in building thermal insulations such as polystyrene (EPS), extruded polystyrene (XPS), Polyurethane (PU) etc. and high energy intensive mineral and rock wool predominately used in construction sector. All these current thermal insulators not only emitted high greenhouse gases, these materials at end of life end up into landfilling or in water bodies. Renewability and sustainability in construction materials driving the ongoing research globally to find alternative solutions to fossil based thermal insulation materials without compromising the insulating material performance requirements.

Lignocellulosic bio-foams have been among the most emerging solutions [57]; and these foams can be produced without the use of synthetic binder or glue by using various processing methods including use of foaming agents or surfactants. The hydrogen bonding between the fine fibres provides the required stability, however the TMP (thermo-mechanical pulp), C-TMP (chemo-thermomechanical pulp), kraft grade fibres or other lignocellulosic fibres does not formed packed hydrogen

bonding like they formed in denser products. Density is the most crucial factor for defining the thermal performance of bio-foams, so for achieving the density and thermal performance, physical hydrogen boding is being formed with the aid of cellulose nanofibers (CNFs), or sodium alginate etc.

As dissipated in Table 10, the produced bio-foams based on different lignocellulosic fibres have used CNFs [59,61] as a main renewable binding agent along with SDS as main surfactant. The density range of these based bio-foams on TMF and CNFs are ranging from 8 to 100 kg/m^3, higher percentage of surfactant reduces the density. Thermal conductivity is ranging between 31 and 43 mW/m.K and the compressive strength is comparable to commercial insulators. In another study [60], micron-size TMP mixed with clay and produced the foam with a density 136 kg/m^3 and thermal conductivity 43.5 43 mW/m.K. Simple hot-pressed rapeseed straw TMP fibre based thermal insulator also produced one study [62] with density ~136 kg/m^3 with a thermal conductivity ~53 mW/m.K. Production of CNFs still is not economically feasible at industrial level [35,64], so it limits the use CNFs in bio-foam production in present situation.

Our present study demonstrated that the reactive extrusion process could be feasible processing technology to large scale production of sub-micron size lignocellulosic fibers and its utilization in bio-foam production. In this work, reeds foams were produced without any physical binding agent such as CNFs or clay. The properties such as density and thermal conductivity of reed foams are comparable to commercial products, and the mechanical properties seem better compared to reported in literature.

Overall, in current situation plant fiber foams are not yet a straightforward drop-in replacement for PU or EPS in performance or cost-critical applications. Their moisture sensitivity, lower thermal resistance, and immature processing infrastructure remain genuine limitations. However, their environmental credentials dramatically lower carbon footprint, biodegradability, and renewable feedstocks are unambiguous advantages that position them strongly as regulatory and market pressures on conventional petrochemical foams intensify. The most promising near-term pathway lies in hybrid systems: incorporating plant fibers as reinforcements within partially bio-based matrices, or targeting niche applications (packaging, low-load insulation) where the environmental benefit is decisive and performance requirements are more easily met.

5. Conclusions

Reactive extrusion of both untreated and PHW-extracted common reed, pioneered in this study, proved to be a successful fiber separation method for foam preparation. Compared to traditional defibration and delignification methods commonly used in the production of bio-based materials, multi-screw reactive extrusion offers a relatively simple, one-step process with several notable advantages. These include reduced energy demand, elimination of expensive or environmentally harmful chemicals, and a continuous operation capability at relatively high solid contents, thereby minimizing water consumption.

The reed foams produced in this study using a simple benchtop method with hydrogen peroxide and SDS demonstrated promising self-bonding properties. The foams exhibited acceptable density and porosity, along with thermal conductivity and mechanical properties comparable to those of commercial insulation materials such as EPS, polyurethane (PU), and cellulose-based products highlighting the considerable potential of common reed as a raw material for thermal insulation applications. The incorporation of moderate amounts of TMP reed fibers further enhanced thermal performance and influenced pore structure and mechanical properties; however, additional research is required to fully confirm, clarify, and explain these effects. Future work should also focus on improving the moisture susceptibility and flame-retardant properties of the reed foams, as these remain critical parameters for practical application. The reactive extrusion process was

Table 10
Survey about the different lignocellulosic binder-less properties bio-foams in the existing literature and comparison with present results along with commercial thermal insulators.

Materials/processing technique	Foaming agent	Density (kg/m3)	Thermal conductivity [mW/m.K)]	Compressive strength (strain%) (kPa)	Tensile strength (kPa)	Ref.
Common reeds, hot-water extraction treated reeds and reactive extrusion, TMP reeds	SDS and H2O2			50% strain		**present work**
	UER1	153.99	50	767.07	46.45	
	UER2	151.81	47	200.4	56.73	
	UER3	189.73	56	1328.8	88.08	
	UER4	120.05	43	252.5	11.16	
	EER1	197.72	36	884	10.77	
	EER2	159.06	43	796.7	59.24	
	EER3	238.49	69	1073.5	14.74	
	EER4	164.25	54	900.4	42.08	
Softwood chemi-thermomechanical pulp (CTMP) mechanical micro-fibrillation using disc milling (MF-CTMP)				50% Strain	-	[58]
	SDS (0 g/L))	89	~42	~30		
	SDS (0.2 g/L)	~20	~36	~0.5		
	SDS (1 g/L)	8.6	~31.1	~0.1		
Thermomechanical pulp fibers (TMP), refined wood fibers (RWF), pine flour (PF) and Cellulose nanofibrils (CNFs)	10% CNF based			25 % strain	-	[59]
	TMP/PF (45/45)	27.5	36.7	1.14		
	TMP/RWF (45/45)	21.50	38.5	1.10		
	TMP/RWF/PF (30/30/30)	25	36.8	1.10		
Pressurized disk milling fibrillation on the surface of refiner mechanical pulp (RMP), clay	[M.RMP 5 wt%-[1 g/L SDS-clay/fiber 2 (w/w)]	136	43.7	25% strain 126	-	[60]
TMP fibres, and CNFs	10% solid content of TMF fiber with 2 g/L SDS and 10% CNF	104	43	25% strain ~200	-	[61]
TMP fibers of rapeseed straw	No-foaming agent			-	-	[62]
	Fine fibers	139	53.3			
	Medium fibers	137	51.9			
	Coarse fibers	135	52.1			
Glass wool (GW)	Commercial product	32.7	34.1	<1 (10% strain)		[57,63]
Rock wool (RW)	Commercial product	39.7	37.6	4-10 (10% strain)		[57,63]
Polystyrene (EPS)	Commercial product	20	42.3	~130 (10% strain)		[57,63]
Wood Fibreboard (WFB)	Commercial product	180	45.8	200 (10% strain)	30	[63], [57]

conducted using a pilot-scale planetary roller extruder (PRE), and processing parameters were systematically optimized throughout this study. Going forward, scalability towards continuous foam production will be explored, including the fabrication of larger reed foam panels to advance the technical readiness level (TRL) and enhance market acceptability.

In terms of potential market opportunities, additional applications such as acoustic insulation and cushioning materials for packaging warrant investigation in future studies, further broadening the commercial prospects of this bio-based foam technology.

Declaration of generative AI use

Authors declared that the no AI or any associate generative AI tools has used in preparation process of this manuscript.

CRediT authorship contribution statement

Ainu Voipio: Data curation, Formal analysis, Investigation, Methodology, Validation, Writing – review & editing. **Veikko Möttönen:** Data curation, Formal analysis, Methodology, Writing – review & editing. **Kristiina Lång:** Funding acquisition, Project administration, Resources, Writing – review & editing. **Tapani Vuorinen:** Methodology, Resources, Supervision, Writing – review & editing. **Anuj Kumar:** Conceptualization, Data curation, Formal analysis, Investigation, Methodology, Resources, Supervision, Validation, Visualization, Writing – original draft, Writing – review & editing.

Declaration of competing interest

The authors declare that they have no known competing financial interests or personal relationships that could have appeared to influence the work reported in this paper.

Acknowledgements

The work is part of FIBSUN project funded by Horizon Europe (grant no. 101112318) and supported by the Circular Bio-based Europe Joint Undertaking and its members. Authors would like acknowledge Dmitry Tarasov from Åbo Akademi for initial planning of PWHE experiment and Edern PHILIPPOT from FCBA for supplying the reeds TMP fibers.

Appendix A. Supplementary data

Supplementary data to this article can be found online at https://doi.org/10.1016/j.mtsust.2026.101383.

Data availability

The data is available on Zenodo: link will be provided.

References

[1] M. Hummel, R. Büchele, A. Müller, E. Aichinger, J. Steinbach, L. Kranzl, et al., The costs and potentials for heat savings in buildings: refurbishment costs and heat saving cost curves for 6 countries in Europe, Energy Build. 231 (2021 Jan) 110454, https://doi.org/10.1016/j.enbuild.2020.110454.

[2] S. Serrano, D. Ürge-Vorsatz, C. Barreneche, A. Palacios, L.F. Cabeza, Heating and cooling energy trends and drivers in Europe, Energy 119 (2017 Jan) 425–434, https://doi.org/10.1016/j.energy.2016.12.080.

[3] L. Pajek, M. Košir, Strategy for achieving long-term energy efficiency of European single-family buildings through passive climate adaptation, Appl. Energy 297 (2021 Sep) 117116, https://doi.org/10.1016/j.apenergy.2021.117116.

[4] U. Berardi, Building energy consumption in US, EU, and BRIC countries, Procedia Eng. 118 (2015) 128–136, https://doi.org/10.1016/j.proeng.2015.08.411.

[5] A. Kumar, K. Stanëk, P. Ryparová, P. Hajek, J. Tywoniak, Hydrophobic treatment of wood fibrous thermal insulator by octadecyltrichlorosilane and its influence on hygric properties and resistance against moulds, Composites, Part B Eng. 106 (2016 Dec) 285–293, https://doi.org/10.1016/j.compositesb.2016.09.034.

[6] M. Chikhi, B. Agoudjil, A. Boudenne, A. Gherabli, Experimental investigation of new biocomposite with low cost for thermal insulation, Energy Build. 66 (2013 Nov) 267–273, https://doi.org/10.1016/j.enbuild.2013.07.019.

[7] A.M. Papadopoulos, State of the art in thermal insulation materials and aims for future developments, Energy Build. 37 (1) (2005 Jan) 77–86, https://doi.org/10.1016/j.enbuild.2004.05.006.

[8] O. Väntsi, T. Kärki, Mineral wool waste in Europe: a review of mineral wool waste quantity, quality, and current recycling methods, J. Mater. Cycles Waste Manag. 16 (1) (2014 Feb) 62–72, https://doi.org/10.1007/s10163-013-0170-5.

[9] J.L. Sohn, P.P. Kalbar, G.T. Banta, M. Birkved, Life-cycle based dynamic assessment of mineral wool insulation in a Danish residential building application, J. Clean. Prod. 142 (2017 Jan) 3243–3253, https://doi.org/10.1016/j.jclepro.2016.10.145.

[10] Z.S. Yap, N.H.A. Khalid, Z. Haron, A. Mohamed, M.M. Tahir, S. Hasyim, et al., Waste mineral wool and its opportunities—A review, Materials 14 (19) (2021 Oct 2) 5777, https://doi.org/10.3390/ma14195777.

[11] M. Schulte, I. Lewandowski, R. Pude, M. Wagner, Comparative life cycle assessment of bio-based insulation materials: environmental and economic performances, GCB Bioenergy 13 (6) (2021 Jun) 979–998, https://doi.org/10.1111/gcbb.12825.

[12] H. Brix, S. Ye, E.A. Laws, D. Sun, G. Li, X. Ding, et al., Large-scale management of common reed, Phragmites australis, for paper production: a case study from the Liaohe Delta, China, Ecol. Eng. 73 (2014 Dec) 760–769, https://doi.org/10.1016/j.ecoleng.2014.09.099.

[13] V. Kočí, M. Jerman, Z. Pavlík, J. Maděra, J. Žák, R. Černý, Interior thermal insulation systems based on wood fiberboards: experimental analysis and computational assessment of hygrothermal and energy performance in the Central European climate, Energy Build. 222 (2020 Sep) 110093, https://doi.org/10.1016/j.enbuild.2020.110093.

[14] E.S. Nouemsi, Z.N.M. Ngouloure, J.C. Bidoung, E. Kamseu, S. Rossignol, C. Leonelli, Dependence of the insulating behavior of some common woods to the pore network and packing density of their fibers: a microstructural approach, Transport Porous Media 138 (2) (2021 Jun) 309–336, https://doi.org/10.1007/s11242-021-01610-5.

[15] F. Segovia, P. Blanchet, N. Auclair, G. Essoua Essoua, Thermo-mechanical properties of a wood fiber insulation board using a bio-based adhesive as a binder, Buildings 10 (9) (2020 Sep 1) 152, https://doi.org/10.3390/buildings10090152.

[16] L. Zampori, G. Dotelli, V. Vernelli, Life cycle assessment of hemp cultivation and use of hemp-based thermal insulator materials in buildings, Environ. Sci. Technol. 47 (13) (2013 Jul 2) 7413–7420, https://doi.org/10.1021/es401326a.

[17] A. Hussain, J. Calabria-Holley, M. Lawrence, Y. Jiang, Hygrothermal and mechanical characterisation of novel hemp shiv based thermal insulation composites, Constr. Build. Mater. 212 (2019 Jul) 561–568, https://doi.org/10.1016/j.conbuildmat.2019.04.029.

[18] B. Gaujena, V. Agapovs, A. Borodinecs, K. Strelets, Analysis of thermal parameters of hemp fiber insulation, Energies 13 (23) (2020 Dec 3) 6385, https://doi.org/10.3390/en13236385.

[19] R. Muthuraj, C. Lacoste, P. Lacroix, A. Bergeret, Sustainable thermal insulation biocomposites from rice husk, wheat husk, wood fibers and textile waste fibers: elaboration and performances evaluation, Ind. Crops Prod. 135 (2019 Sep) 238–245, https://doi.org/10.1016/j.indcrop.2019.04.053.

[20] N.A. Ramlee, J. Naveen, M. Jawaid, Potential of oil palm empty fruit bunch (OPEFB) and sugarcane bagasse fibers for thermal insulation application – a review, Constr. Build. Mater. 271 (2021 Feb) 121519, https://doi.org/10.1016/j.conbuildmat.2020.121519.

[21] M. Sammul, K. Kauer, T. Köster, Biomass accumulation during reed encroachment reduces efficiency of restoration of B altic coastal grasslands, in: N. Hölzel (Ed.), Appl. Veg. Sci. 15 (2) (2012 Apr) 219–230, https://doi.org/10.1111/j.1654-109X.2011.01167.x.

[22] S. Rasool, T. Rasool, K.M. Gani, Unlocking the potential of wetland biomass: treatment approaches and sustainable resource management for enhanced utilization, Bioresour. Technol. Rep. 23 (2023 Sep) 101553, https://doi.org/10.1016/j.biteb.2023.101553.

[23] F. Gröndahl, N. Brandt, S. Karlsson, M.E. Malmström, Sustainable use of Baltic Sea natural resources based on ecological engineering and biogas production, in: Chianciano Terme, Italy, 2009, pp. 153–161, https://doi.org/10.2495/ECO090151 [cited 2023 Oct 29], http://library.witpress.com/viewpaper.asp?pcode=ECO09-015-1.

[24] T. Avellán, P. Gremillion, Constructed wetlands for resource recovery in developing countries, Renew. Sustain. Energy Rev. 99 (2019 Jan) 42–57, https://doi.org/10.1016/j.rser.2018.09.024.

[25] I. Gelfand, R. Sahajpal, X. Zhang, R.C. Izaurralde, K.L. Gross, G.P. Robertson, Sustainable bioenergy production from marginal lands in the US Midwest, Nature 493 (7433) (2013 Jan) 514–517, https://doi.org/10.1038/nature11811.

[26] J.M. Allirand, G. Gosse, An above-ground biomass production model for a common reed (Phragmites communis Trin.) stand, Biomass Bioenergy 9 (6) (1995 Jan) 441–448, https://doi.org/10.1016/0961-9534(95)00042-9.

[27] T.K. Mal, L. Narine, The biology of Canadian weeds. 129. *Phragmites australis* (Cav.) Trin. ex Steud, Can. J. Plant Sci. 84 (1) (2004 Jan 1) 365–396, https://doi.org/10.4141/P01-172.

[28] J.F. Köbbing, N. Thevs, S. Zerbe, The utilisation of reed (Phragmites australis): a review, Mires Peat [Internet] 13 (1) (2013 Oct 14). Available from: http://mires-and-peat.net/pages/volumes/map13/map1301.php.

[29] L. Zampori, G. Dotelli, V. Vernelli, Life cycle assessment of hemp cultivation and use of hemp-based thermal insulator materials in buildings, Environ. Sci. Technol. 47 (13) (2013 Jul 2) 7413–7420, https://doi.org/10.1021/es401326a.

[30] B. Gaujena, V. Agapovs, A. Borodinecs, K. Strelets, Analysis of thermal parameters of hemp fiber insulation, Energies 13 (23) (2020 Dec 3) 6385, https://doi.org/10.3390/en13236385.
[31] R. Zhao, H. Guo, X. Yi, W. Gao, H. Zhang, Y. Bai, et al., Research on thermal insulation properties of plant fiber composite building material: a review, Int. J. Thermophys. 41 (6) (2020 Jun) 87, https://doi.org/10.1007/s10765-020-02665-0.
[32] D. Csanády, O. Fenyvesi, B. Nagy, Heat transfer in straw-based thermal insulating materials, Materials 14 (16) (2021 Aug 6) 4408, https://doi.org/10.3390/ma14164408.
[33] B. Theobald, A. Tay, S. Ranganathan, Q. Tanjay, S. Patel, R. Van Leeuwen, et al., Thermomechanical biorefining of Pinus radiata biomass to produce biochemicals using reactive extrusion, Bioresour Bioprocess 12 (1) (2025 Nov 5) 131, https://doi.org/10.1186/s40643-025-00971-9.
[34] T.T.T. Ho, K. Abe, T. Zimmermann, H. Yano, Nanofibrillation of pulp fibers by twin-screw extrusion, Cellulose 22 (1) (2015 Feb) 421–433, https://doi.org/10.1007/s10570-014-0518-6.
[35] G. Signori-Iamin, R.J. Aguado, J.L. Putaux, A.F. Santos, W. Thielemans, M. Delgado-Aguilar, Energy and property trade-offs in nanocellulose production: high-pressure homogenization at different processing consistencies, Chem. Eng. J. 509 (2025 Apr) 161257, https://doi.org/10.1016/j.cej.2025.161257.
[36] K. Albrecht, F. Neudecker, S. Veigel, S. Bodner, J. Keckes, W. Gindl-Altmutter, The suitability of common reed (Phragmites australis) for load-bearing structural materials, J. Mater. Sci. 58 (39) (2023 Oct) 15411–15420, https://doi.org/10.1007/s10853-023-08996-1.
[37] A. Mittal, T.B. Vinzant, R. Brunecky, S.K. Black, H.M. Pilath, M.E. Himmel, et al., Investigation of the role of lignin in biphasic xylan hydrolysis during dilute acid and organosolv pretreatment of corn stover, Green Chem. 17 (3) (2015) 1546–1558, https://doi.org/10.1039/C4GC02258K.
[38] P. Giri, C. Tambe, R. Narayan, Using reactive extrusion to manufacture greener products: from laboratory fundamentals to commercial scale, in: A. Ayoub, L. Lucia (Eds.), ACS Symposium Series [Internet], American Chemical Society, Washington, DC, 2018, pp. 1–23, https://doi.org/10.1021/bk-2018-1304.ch001 [cited 2025 Feb 24], https://pubs.acs.org/doi/abs/10.1021/bk-2018-1304.ch001.
[39] M. Mascarenhas, J. Dighton, G.A. Arbuckle, Characterization of plant carbohydrates and changes in leaf carbohydrate chemistry due to chemical and enzymatic degradation measured by microscopic ATR FT-IR spectroscopy, Appl. Spectrosc. 54 (5) (2000 May) 681–686, https://doi.org/10.1366/0003702001950166.
[40] X. Wang, Y. Deng, S. Wang, C. Liao, Y. Meng, T. Pham, Nanoscale characterization of reed stalk fiber cell walls, Bioresources 8 (2) (2013 Feb 26) 1986–1996, https://doi.org/10.15376/biores.8.2.1986-1996.
[41] P. Pandiarajan, M. Kathiresan, Physicochemical and mechanical properties of a novel fiber extracted from the stem of common reed plant, Int. J. Polym. Anal. Char. 23 (5) (2018 Jul 4) 442–449, https://doi.org/10.1080/1023666X.2018.1474327.
[42] Barman D. Nath, MdA. Haque, T.H. Kang, G.H. Kim, T.Y. Kim, M.K. Kim, et al., Effect of mild alkali pretreatment on structural changes of reed (*Phragmites communis* Trinius) straw, Environ. Technol. 35 (2) (2014 Jan 17) 232–241, https://doi.org/10.1080/09593330.2013.824009.
[43] Y. Jiao, C. Wan, T. Qiang, J. Li, Synthesis of superhydrophobic ultralight aerogels from nanofibrillated cellulose isolated from natural reed for high-performance adsorbents, Appl. Phys. A 122 (7) (2016 Jul) 686, https://doi.org/10.1007/s00339-016-0194-5.
[44] Anh LD. Hung, Z. Pásztory, An overview of factors influencing thermal conductivity of building insulation materials, J. Build. Eng. 44 (2021 Dec) 102604, https://doi.org/10.1016/j.jobe.2021.102604.
[45] J. Zach, R. Slávik, V. Novák, Investigation of the process of heat transfer in the structure of thermal insulation materials based on natural fibres, Procedia Eng. 151 (2016) 352–359, https://doi.org/10.1016/j.proeng.2016.07.389.
[46] J. Zach, A. Korjenic, V. Petránek, J. Hroudová, T. Bednar, Performance evaluation and research of alternative thermal insulations based on sheep wool, Energy Build. 49 (2012 Jun) 246–253, https://doi.org/10.1016/j.enbuild.2012.02.014.
[47] Sulong NH. Ramli, S.A.S. Mustapa, M.K. Abdul Rashid, Application of expanded polystyrene (EPS) in buildings and constructions: a review, J. Appl. Polym. Sci. 136 (20) (2019 May 20) 47529, https://doi.org/10.1002/app.47529.
[48] Y. Li, Y. Sun, J. Qiu, T. Liu, L. Yang, H. She, Moisture absorption characteristics and thermal insulation performance of thermal insulation materials for cold region tunnels, Constr. Build. Mater. 237 (2020 Mar) 117765, https://doi.org/10.1016/j.conbuildmat.2019.117765.
[49] K.W. Euliss, B.L. Dorsey, K.C. Benke, M.K. Banks, A.P. Schwab, The use of plant tissue silica content for estimating transpiration, Ecol. Eng. 25 (4) (2005 Nov) 343–348, https://doi.org/10.1016/j.ecoleng.2005.06.003.
[50] L.A. Zemnukhova, A.E. Panasenko, A.P. Artem'yanov, E.A. Tsoy, Dependence of porosity of amorphous silicon dioxide prepared from rice straw on plant variety, Bioresources 10 (2) (2015 Apr 29) 3713–3723, https://doi.org/10.15376/biores.10.2.3713-3723.
[51] R. Ellerbrock, M. Stein, J. Schaller, Comparing amorphous silica, short-range-ordered silicates and silicic acid species by FTIR, Sci. Rep. 12 (1) (2022 Jul 9) 11708, https://doi.org/10.1038/s41598-022-15882-4.
[52] K.M. Chen, F. Wang, Y.H. Wang, T. Chen, Y.X. Hu, J.X. Lin, Anatomical and chemical characteristics of foliar vascular bundles in four reed ecotypes adapted to different habitats, Flora - Morphol Distrib Funct Ecol Plants 201 (7) (2006 Oct) 555–569, https://doi.org/10.1016/j.flora.2005.12.003.
[53] L.M. Matuana, J.J. Balatinecz, R.N.S. Sodhi, C.B. Park, Surface characterization of esterified cellulosic fibers by XPS and FTIR Spectroscopy, Wood Sci. Technol. 35 (3) (2001 Jun 1) 191–201, https://doi.org/10.1007/s002260100097.
[54] B.V.M. Rodrigues, E. Heikkilä, E. Frollini, P. Fardim, Multi-technique surface characterization of bio-based films from sisal cellulose and its esters: a FE-SEM, μ-XPS and ToF-SIMS approach, Cellulose 21 (3) (2014 Jun) 1289–1303, https://doi.org/10.1007/s10570-014-0216-4.
[55] X.Y. Huang, C.F. De Hoop, X.P. Peng, J.L. Xie, J.Q. Qi, Y.Z. Jiang, et al., Thermal stability analysis of polyurethane foams made from microwave liquefaction bio-polyols with and without solid residue, Bioresources 13 (2) (2018 Mar 15) 3346–3361, https://doi.org/10.15376/biores.13.2.3346-3361.
[56] X. Wang, J. Jang, Y. Su, J. Liu, H. Zhang, Z. He, et al., Starting materials, processes and characteristics of bio-based foams: a review, J. Bioresour. Bioprod. 9 (2) (2024 May) 160–173, https://doi.org/10.1016/j.jobab.2024.01.004.
[57] Anh LD. Hung, Z. Pásztory, An overview of factors influencing thermal conductivity of building insulation materials, J. Build. Eng. 44 (2021 Dec) 102604, https://doi.org/10.1016/j.jobe.2021.102604.
[58] Y. Zhu, J. Zhu, Z. Yu, Y. Ye, X. Sun, Y. Zhang, et al., Air drying scalable production of hydrophobic, mechanically stable, and thermally insulating lignocellulosic foam, Chem. Eng. J. 450 (2022 Dec) 138300, https://doi.org/10.1016/j.cej.2022.138300.
[59] Hajam M. El, W. Sun, R. Hossain, I. Hafez, C. Howell, M. Tajvidi, Surfactant-assisted foam-forming of high performance ultra-low density structures made from lignocellulosic materials and cellulose nanofibrils (CNFs), Ind. Crops Prod. 221 (2024 Dec) 119357, https://doi.org/10.1016/j.indcrop.2024.119357.
[60] Y. Zhu, J. Zhu, Y. Li, J. Chen, O. Rojas, F. Jiang, Chemical binder-free and oven-dried Lignocellulose/clay composite foams: flame resistance, thermal insulation, and recyclability, ACS Sustain. Chem. Eng. 11 (46) (2023 Nov 20) 16499–16508, https://doi.org/10.1021/acssuschemeng.3c04108.
[61] R. Hossain, M. El Hajam, I. Hafez, M. Tajvidi, Structure-property insights into foam-forming processing of lignocellulosic materials, Constr. Build. Mater. 489 (2025 Aug) 142401, https://doi.org/10.1016/j.conbuildmat.2025.142401.
[62] M. Jerman, M. Böhm, J. Vrzáň, J. Krejsová, K. Kobetičová, R. Černý, Binderless thermal insulation boards from rapeseed straw: optimization and performance analysis, Materials 18 (24) (2025 Dec 5) 5481, https://doi.org/10.3390/ma18245481.
[63] D. Kumar, M. Alam, P.X.W. Zou, J.G. Sanjayan, R.A. Memon, Comparative analysis of building insulation material properties and performance, Renew. Sustain. Energy Rev. 131 (2020 Oct) 110038, https://doi.org/10.1016/j.rser.2020.110038.
[64] S. Garg, A. Avanthi, Overcoming cost, energy, and process barriers for industrially viable nanocellulose production, Discov. Appl. Sci. 7 (11) (2025 Oct 21) 1262, https://doi.org/10.1007/s42452-025-07650-6.